INTERNATIONAL JOURNAL FOR NUMERICAL METHODS IN FLUIDS, VOL. 18, 575–604 (1994)

A SECOND-ORDER RADIATION BOUNDARY CONDITION FOR THE SHALLOW WATER WAVE EQUATIONS ON TWO-DIMENSIONAL UNSTRUCTURED FINITE ELEMENT GRIDS

MATTHIAS JOHNSEN AND DANIEL R. LYNCH

Thayer School of Engineering, Dartmouth College, Hanover, NH 03755, U.S.A.

SUMMARY

A second-order radiation boundary condition (RBC) is derived for 2D shallow water problems posed in 'wave equation' form and is implemented within the Galerkin finite element framework. The RBC is derived by matching the dispersion relation for the interior wave equation with an approximate solution to the exterior problem for outgoing waves. The matching is correct to second order, accounting for curvature of the wave front and the geometry. Implementation is achieved by using the RBC as an evolution equation for the normal gradient on the boundary, coupled through the natural boundary integral of the Galerkin interior problem. The formulation is easily implemented on non-straight, unstructured meshes of simple elements. Test cases show fidelity to solutions obtained on extended meshes and improvement relative to simpler first-order RBCs.

KEY WORDS Radiation boundary conditions Open boundary conditions Shallow water wave equations Sommerfeld condition Klein–Gordon equation

1. INTRODUCTION

In a number of computational solutions of wave propagation problems the domain of interest has to be terminated artificially in order to limit the computational expenses. On such open boundaries there is a need for the specification of some sort of boundary condition that allows signals (waves) emanating within the domain to exit through the boundary as if it were not present. Several approaches have been devised for the treatment of open boundaries. Review papers were compiled e.g. by Chapman,[1] Moore *et al.*[2] and most recently by Givoli.[3] Early approaches include the use of sponge zones[1] and so-called infinite elements.[4] Exact methods for the treatment of the open boundary include the hybrid method developed by Lynch *et al.*,[5] coupling an interior finite element formulation with a boundary element formulation for the exterior, and the global look-back truncation scheme of Ziolkowski *et al.*[6] These formulations are non-local in space and/or time and hence computationally expensive, but they are feasible for some problems.

As a formulation that is local in both space and time, the use of radiation boundary conditions (RBCs) has found widespread acceptance. The approach is based on an approximate form of the governing partial differential equation (PDE) which is applied at the open boundary. The simplest form is the Sommerfeld condition,[7] which is exact for the one-dimensional, pure wave equation. Several methods have been devised to implement this condition in finite difference codes (see e.g. References 1 and 8). Boundary conditions for multidimensional problems have

CCC 0271–2091/94/060575–30

Received 7 January 1993
Revised 5 October 1993

been derived e.g. by Engquist and Majda,[9] Bayliss and Turkell,[10] Feng[11] and Higdon.[12] It has been common to distinguish approximations of various orders, with the Sommerfeld condition being a first-order condition.

Most studies deal with the 'pure' wave equation, but several authors have studied open boundary conditions for more generalized PDEs. For example, Engquist and Majda[9] and Verboom and Slob[13] have considered the shallow water equations and Johnsen *et al.*[14] have studied RBCs for the one-dimensional telegraph and Klein–Gordon equations. Other examples are given in Reference 3.

The present study provides a derivation of a new second-order RBC for shallow water problems with rotation. Its implementation in two-dimensional finite element codes is shown, including the treatment of curved boundaries and irregular meshes. The study shows the quality of the RBC for the pure wave equation, the shallow water wave equation as formulated by Lynch and Gray[15] and the Klein–Gordon equation.

GOVERNING EQUATIONS

The shallow water equations in their simplest form are

$$\frac{\partial \zeta}{\partial t} + \frac{\partial (hu)}{\partial x} + \frac{\partial (hv)}{\partial y} = 0, \tag{1}$$

$$\frac{\partial u}{\partial t} - fv + g\frac{\partial \zeta}{\partial x} = 0, \tag{2}$$

$$\frac{\partial v}{\partial t} + fu + g\frac{\partial \zeta}{\partial y} = 0, \tag{3}$$

where ζ is the free surface elevation, h is the water depth, u and v are the velocities in the x- and y-direction respectively, f is the Coriolis parameter and g is the gravitational acceleration. The effects of friction, wind forcing, baroclinicity and advection are neglected. This system of equations can be reformulated to yield the elevation equation in two different wave equation forms. Following Lynch and Gray,[15] we obtain the shallow water wave equation (SWWE)

$$\frac{\partial^2 \zeta}{\partial t^2} - \nabla \cdot c^2 \nabla \zeta - \nabla \cdot (\mathbf{f} \times h\mathbf{v}) = 0, \tag{4}$$

where $c = \sqrt{(gh)}$ is the wave speed. In the following we assume the water depth h to be constant, in which case it is convenient to restate the SWWE as

$$\frac{\partial^2 \zeta}{\partial t^2} - \nabla \cdot c^2 \nabla \zeta + fh\xi = 0, \tag{5}$$

where the vorticity is introduced as

$$\xi = \frac{\partial v}{\partial x} - \frac{\partial u}{\partial y}. \tag{6}$$

It is easy to show from (1)–(3) that

$$\frac{\partial}{\partial t}(f\zeta - h\xi) = 0, \tag{7}$$

which can be stated as

$$Q'(x, y) = \frac{\xi}{h} - \frac{f\zeta}{h^2} = \frac{\xi(x, y, t = 0)}{h} - \frac{f\zeta(x, y, t = 0)}{h^2} \tag{8}$$

where $Q'(x, y)$ is the perturbation potential vorticity. This leads to the Klein–Gordon equation (KGE) (see e.g. Reference 16)

$$\frac{\partial^2 \zeta}{\partial t^2} - \nabla \cdot c^2 \nabla \zeta + f^2 \zeta = -fh^2 Q'(x, y). \tag{9}$$

Both of these wave equations (4) and (9) will be used herein. The SWWE requires simultaneous solution of (2) and (3) for the velocities in the rotational term; the KGE is uncoupled from the velocities. In the absence of rotation they are of course identical and reduce to the 'pure' wave equation.

DERIVATION OF THE RADIATION BOUNDARY CONDITION

Several methods have been used for the derivation of RBCs. Our derivation is based on the dispersion relation of the Klein–Gordon equation.

We assume for simplicity that the initial conditions are such that the potential vorticity Q' is zero on the boundary. In this case the KGE can be rewritten in (approximate) cylindrical co-ordinates as

$$\frac{\partial^2 \zeta}{\partial t^2} - c^2 \left(\frac{\partial^2 \zeta}{\partial r^2} + \frac{1}{r} \frac{\partial \zeta}{\partial r} + \frac{\partial^2 \zeta}{\partial s^2} \right) + f^2 \zeta = 0. \tag{10}$$

Following Johnsen *et al.*,[14] we consider the solution of the form

$$\zeta = \zeta_0 e^{j(-\omega t + \kappa_s s)} H_0^{(1)}(\kappa_n r), \tag{11}$$

where ζ_0 is a constant, $H_0^{(1)}$ is the Hankel function of zeroth order, ω is a frequency and κ_n and κ_s are the wave numbers in the normal and tangential direction respectively. This solution yields the dispersion relation

$$-\omega^2 + c^2(\kappa_n^2 + \kappa_s^2) + f^2 = 0. \tag{12}$$

This dispersion relation is now solved for κ_n, where we consider two limiting cases. In the first case we assume that $\omega \gg f$, so that

$$\kappa_n = \pm \frac{\omega}{c} \sqrt{\left(1 - \frac{c^2}{\omega^2} \kappa_s^2 \right)}. \tag{13}$$

The square-root term is now linearized, where linearizations of different order can be used. We employ a second-order linearization of the square-root term which consists of the approximation

$$\sqrt{(1 - \chi)} \approx p_0 - p_2 \chi. \tag{14}$$

The coefficients p_0 and p_2 depend on the type of linearization. For example, a Padé approximation (used herein) gives $p_0 = 1$ and $p_2 = 0{\cdot}5$ (see e.g. Reference 2). This yields the approximate dispersion relation

$$\omega\kappa_n = p_0 \frac{\omega^2}{c} - p_2 c\kappa_s^2 \tag{15}$$

(where we consider only outgoing waves).

In the other limit we assume $f \gg \omega$, so that

$$\kappa_n = \pm j \frac{f}{c} \sqrt{\left(1 + \frac{c^2}{f^2} \kappa_s^2\right)}. \tag{16}$$

Using the same linearization as above, this limit is approximated as

$$jf\kappa_n = -p_0 \frac{f^2}{c} - p_2 c\kappa_s^2. \tag{17}$$

A composite of (15) and (17) which satisfies both asymptotic limits is

$$(\omega + jf)\kappa_n = \frac{p_0}{c}(\omega^2 - f^2) - p_2 c\kappa_s^2. \tag{18}$$

Figures 1 and 2 show the dimensionless normal wave number $c\kappa_n/\omega$ as a function of f/ω in comparison with the exact normal wave number (equation (12)). An additional parameter is the tangential wave number, given in dimensionless form as $c\kappa_s/\omega$. This wave number is directly related to the angle of incidence at which a wave hits a boundary (for the pure wave equation $c\kappa_s/\omega = 0$ corresponds to normal and $c\kappa_s/\omega = 1$ to tangential incidence). Plotted are the amplitude and phase of $c\kappa_n/\omega$ versus f/ω for both dispersion relationships (12) and (18) using $c\kappa_s/\omega = 0$ (Figures 1(a) and 1(b)) and $c\kappa_s/\omega = 0{\cdot}75$ (Figures 2(a) and 2(b)). The plots clearly indicate the validity of the approximation (18), which is asymptotically correct for $f/\omega \to 0$ and $f/\omega \to \infty$.

We now employ the far-field approximation to the exact solution of the wave equation, which fulfils the Sommerfeld condition of radiation (Reference 7, p. 230ff):

$$\zeta = \zeta_0 r^{-1/2} e^{j(-\omega t + \kappa_n r + \kappa_s s)}. \tag{19}$$

Using this solution, we can identify the approximate dispersion relation as being appropriate for the PDE

$$\left(\frac{\partial}{\partial t} + f\right)\frac{\partial \zeta}{\partial n} = -\frac{p_0}{c}\left(\frac{\partial^2}{\partial t^2} + f^2\right)\zeta + p_2 c \frac{\partial^2 \zeta}{\partial s^2} - \frac{1}{2r}\left(\frac{\partial}{\partial t} + f\right)\zeta. \tag{20}$$

This is the desired RBC, expressed as an evolution equation for $\partial\zeta/\partial n$. We will test this in comparison with the Sommerfeld RBC

$$\frac{\partial \zeta}{\partial n} = -\frac{1}{c}\frac{\partial \zeta}{\partial t}, \tag{21}$$

which has been widely studied.

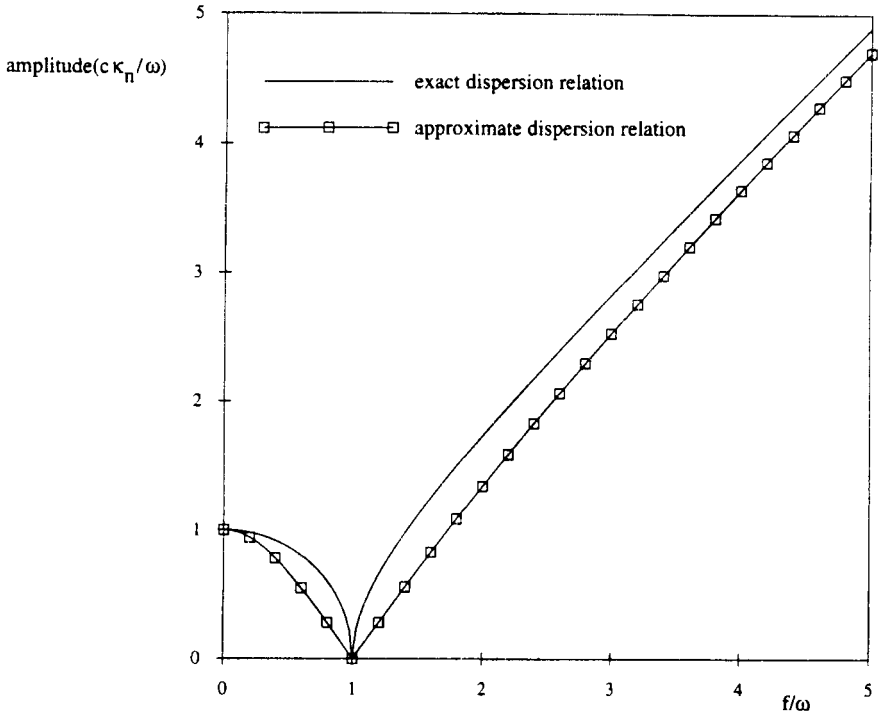

Figure 1(a). Amplitude of the normalized normal wave number $c\kappa_n/\omega$ as a function of f/ω for $c\kappa_s/\omega = 0$

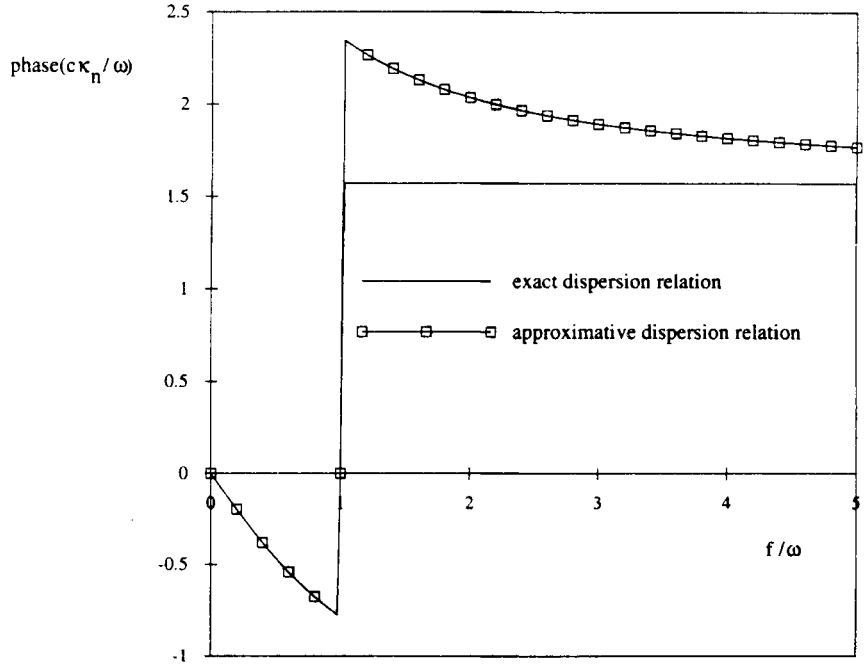

Figure 1(b). Phase of the normalized normal wave number $c\kappa_n/\omega$ as a function of f/ω for $c\kappa_s/\omega = 0$

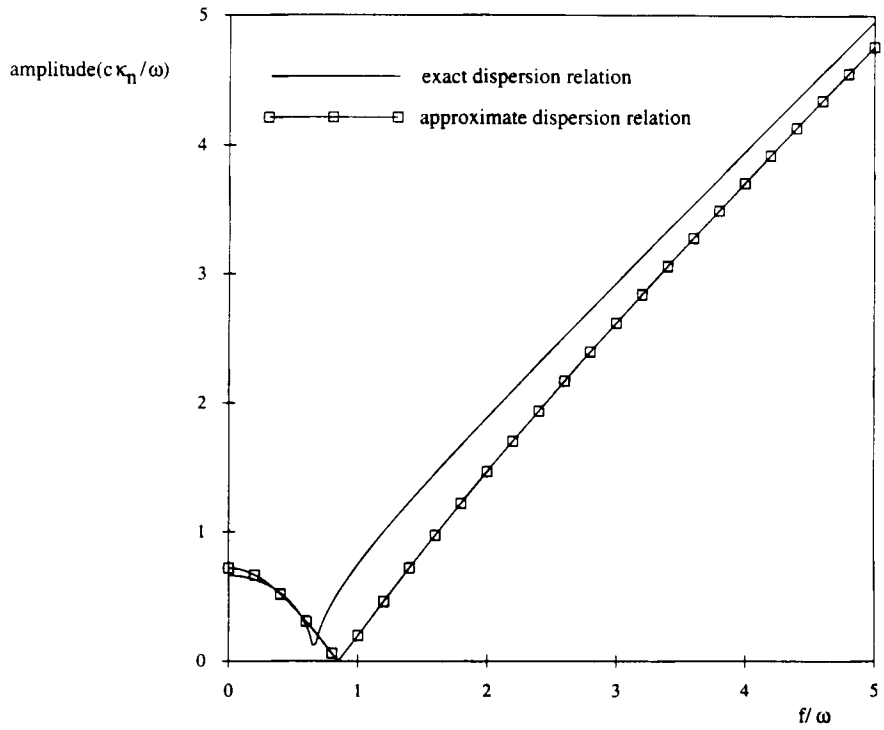

Figure 2(a). Amplitude of the normalized normal wave number $c\kappa_n/\omega$ as a function of f/ω for $c\kappa_s/\omega = 0{\cdot}75$

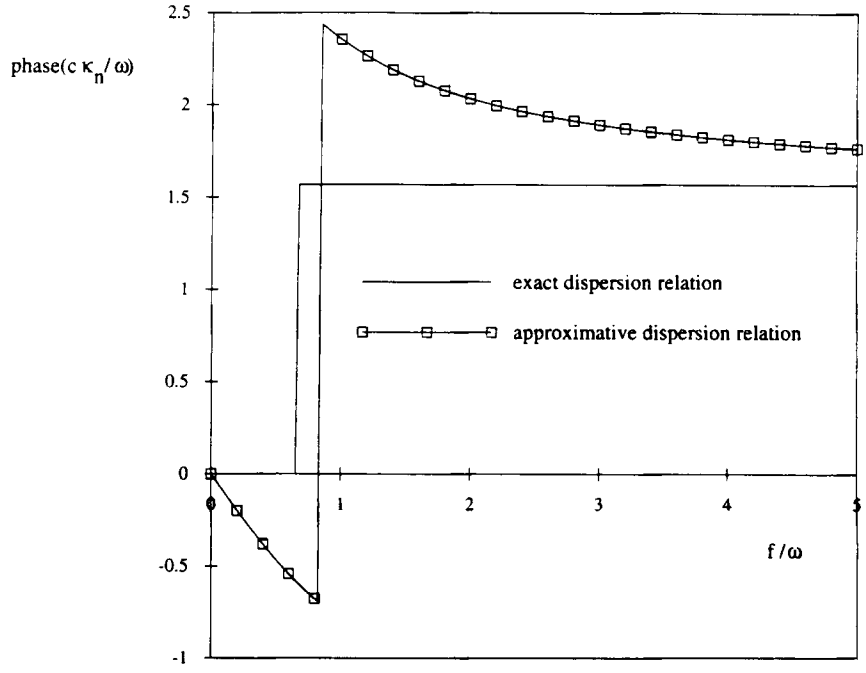

Figure 2(b). Phase of the normalized normal wave number $c\kappa_n/\omega$ as a function of f/ω for $c\kappa_s/\omega = 0{\cdot}75$

FINITE ELEMENT FORMULATION

KGE formulation

The finite element formulation for the KGE is based on the weighted residual statement of equation (9):

$$\left\langle \frac{\partial^2 \zeta}{\partial t^2}, \phi_i \right\rangle - \langle \nabla \cdot c^2 \nabla \zeta, \phi_i \rangle + \langle f^2 \zeta, \phi_i \rangle = \langle -fH^2 Q', \phi_i \rangle, \tag{22}$$

where ϕ_i is a scalar weighting function. The notation $\langle a, b \rangle$ refers to the inner product operator (the integral over the domain of interest of the product of a and b). Integration of the second term by parts results in the weak form

$$\left\langle \frac{\partial^2 \zeta}{\partial t^2}, \phi_i \right\rangle + \langle c^2 \nabla \zeta, \nabla \phi_i \rangle + \langle f^2 \zeta, \phi_i \rangle = \langle -fH^2 Q', \phi_i \rangle + \oint c^2 q \phi_i \, \mathrm{d}s, \tag{23}$$

where the surface integral is evaluated on the boundary of the domain and $q \equiv \partial \zeta / \partial n$ is the normal gradient on the boundary, directed outwards.

Equation (23) is the standard evolution equation for ζ, which is well posed when q is known in the boundary integral (or, alternatively, if ζ is known). For an open boundary neither ζ nor q will be known *a priori*. Instead, we invoke an evolution equation for the normal gradient in the form of the RBC (20). In weak (i.e. boundary integral) form we have

$$\oint \left(\frac{\partial}{\partial t} + f \right) q \phi_i \, \mathrm{d}s = -\oint \frac{p_0}{c} \frac{\partial^2 \zeta}{\partial t^2} \phi_i \, \mathrm{d}s - \oint \frac{p_0}{c} f^2 \zeta \phi_i \, \mathrm{d}s$$
$$- \oint p_2 c \frac{\partial \zeta}{\partial s} \frac{\partial \phi_i}{\partial s} \, \mathrm{d}s - \oint \frac{1}{2\mathrm{r}} \frac{\partial \zeta}{\partial t} \phi_i \, \mathrm{d}s - \oint \frac{f}{2r} \zeta \phi_i \, \mathrm{d}s, \tag{24}$$

wherein the $\partial^2 \zeta / \partial s^2$ term has been integrated by parts.* Equations (23) and (24) define a closed system of two unknown functions: $\zeta(x, y, t)$ on the domain and $q(s, t)$ on the boundary. We expand both functions in the finite element basis ϕ_i:

$$\zeta(x, y, t) = \sum_i \zeta_i(t) \phi_i(x, y), \tag{25}$$

$$q(s, t) = \sum_i q_i(t) \phi_i(s). \tag{26}$$

The isolated role of q in both equations (23) and (24) instantly suggests a semi-implicit time-stepping strategy, which is explored below.

SWWE formulation

The weighted residual statement of the SWWE (4) is given by

$$\left\langle \frac{\partial^2 \zeta}{\partial t^2}, \phi_i \right\rangle - \langle \nabla \cdot c^2 \nabla \zeta, \phi_i \rangle - \langle \nabla \cdot (\mathbf{f} \times h\mathbf{v}), \phi_i \rangle = 0. \tag{27}$$

* A simply closed radiating boundary is assumed. For mixed boundary conditions, endpoint contributions would appear from the integration by parts along a radiating boundary segment (see Appendix).

Integration by parts results in the weak form

$$\left\langle \frac{\partial^2 \zeta}{\partial t^2}, \phi_i \right\rangle + \tau_0 \left\langle \frac{\partial \zeta}{\partial t}, \phi_i \right\rangle + \langle c^2 \nabla \zeta, \nabla \phi_i \rangle + \langle (\mathbf{f} \times h\mathbf{v}) \cdot \nabla \phi_i \rangle$$
$$= \oint c^2 q \phi_i \, ds - \oint \tau_0 (H\mathbf{v}) \cdot \hat{\mathbf{n}} \phi_i \, ds - \oint f h \mathbf{v} \cdot \hat{\mathbf{s}} \phi_i \, ds, \quad (28)$$

in which the additional circulation integral appears on the right-hand side. Here we also introduce the arbitrary factor τ_0 as suggested by Kinnmark and Gray.[17] This factor, which is set to $\tau_0 = 10^{-4}\,\mathrm{s}^{-1}$ stabilizes long-time drifts that otherwise may develop in the solution. The weak form of the RBC (20) is the same as for the KGE formulation (equation (24)). While the KGE formulation is uncoupled from the velocity solution $\mathbf{v}$, the SWWE is not. Hence we need to specify the basis for $\mathbf{v}$, i.e.

$$\mathbf{v}(x, y, t) = \sum_i \mathbf{v}_i(t) \phi_i(x, y), \quad (29)$$

in addition to that for ζ and q (equations (25) and (26)). This basis is used in (24) and (28) and in addition in a Galerkin form of (2) and (3) which is used for the evolution of $\mathbf{v}$ (see below).

IMPLEMENTATION OF THE RBC

KGE formulation

Equation (23) may be discretized in time in a standard manner (see e.g. Reference 15), leading to the form

$$[A]\{\zeta\}^{k+1} = \{b\}^k + \left\{ \oint c^2 \left(\frac{\theta}{2} (q^{k+1} + q^{k-1}) + (1 - \theta) q^k \right) \phi_i \, ds \right\} \quad (30)$$

where superscripts indicate the time level, A is a blend of conventional Laplacian and mass matrices, $\{b\}$ is the vector of known quantities and the boundary integral is centred and implicit. θ is a time-weighting factor, normally set between 0 and 1. We insert the evolution equation of the normal gradient q into the boundary integral as follows. Centred (leapfrog) differencing of (24) leads to

$$\oint \left(\frac{1}{2\Delta t} (q^{k+1} - q^{k-1}) + \frac{\varepsilon f}{2} (q^{k+1} + q^{k-1}) + (1 - \varepsilon) f q^k \right) \phi_i \, ds$$
$$= - \oint \frac{p_0}{c \Delta t^2} (\zeta^{k+1} - 2\zeta^k + \zeta^{k-1}) \phi_i \, ds - \oint \frac{p_0}{c} f^2 \left(\frac{\varepsilon}{2} (\zeta^{k+1} + \zeta^{k-1}) + (1 - \varepsilon) \zeta^k \right) \phi_i \, ds$$
$$- \oint p_2 c \frac{\partial \zeta^k}{\partial s} \frac{\partial \phi_i}{\partial s} \, ds - \oint \frac{1}{4r\Delta t} (\zeta^{k+1} - \zeta^{k-1}) \phi_i \, ds$$
$$- \oint \frac{f}{2r} \left(\frac{\varepsilon}{2} (\zeta^{k+1} + \zeta^{k-1}) + (1 - \varepsilon) \zeta^k \right) \phi_i \, ds, \quad (31)$$

where ε is another time-weighting factor, again usually set between 0 and 1. Rearrangement yields

$$\oint q^{k+1}(1 + f\varepsilon\Delta t)\phi_i \, ds$$
$$= \oint \left[q^{k-1}(1 - f\varepsilon\Delta t) - q^k[2f(1 - \varepsilon)\Delta t] - \zeta^{k+1}\left(\frac{2p_0}{c\Delta t} + \frac{p_0\varepsilon\Delta t f^2}{c} + \frac{1 + f\varepsilon\Delta t}{2r}\right) \right.$$
$$\left. + \zeta^k\left(\frac{4p_0}{c\Delta t} - \frac{2p_0(1 - \varepsilon)\Delta t f^2}{c} - \frac{f(1 - \varepsilon)\Delta t}{r}\right) - \zeta^{k-1}\left(\frac{2p_0}{c\Delta t} + \frac{p_0\varepsilon\Delta t f^2}{c} - \frac{1 - f\varepsilon\Delta t}{2r}\right)\right]\phi_i \, ds$$
$$- \oint 2p_2 c\Delta t \frac{\partial\zeta^k}{\partial s}\frac{\partial\phi_i}{\partial s} \, ds. \tag{32}$$

Insertion of the expanded RBC (32) into the FE boundary integral (30) then yields

$$[A]\{\zeta\}^{k+1} + \oint \frac{c^2\theta}{1 + f\varepsilon\Delta t}\zeta^{k+1}\left(\frac{p_0}{c\Delta t} + \frac{p_0\varepsilon\Delta t f^2}{2c} + \frac{1 + f\varepsilon\Delta t}{4r}\right)\phi_i \, ds$$
$$= \{b\}^k + \oint \frac{c^2}{1 + f\varepsilon\Delta t}\left[[1 - \theta + f(\varepsilon - \theta)\Delta t]q^k + \theta q^{k-1}\right.$$
$$\left. + \theta\zeta^k\left(\frac{2p_0}{c\Delta t} - \frac{p_0(1 - \varepsilon)\Delta t f^2}{c} - \frac{f(1 - \varepsilon)\Delta t}{2r}\right) - \theta\zeta^{k-1}\left(\frac{p_0}{c\Delta t} + \frac{p_0\varepsilon\Delta t f^2}{2c} - \frac{1 - f\varepsilon\Delta t}{4r}\right)\right]\phi_i \, ds$$
$$- \oint \frac{\theta c^3 p_2\Delta t}{1 + f\varepsilon\Delta t}\frac{\partial\zeta^k}{\partial s}\frac{\partial\phi_i}{\partial s} \, ds, \tag{33}$$

where the term in the boundary integral involving ζ^{k+1} is implicit and is moved into the left-hand-side matrix. In the solution procedure the first step is the determination of the boundary integrals (see Appendix). Equation (33) is then assembled and the solution for ζ^{k+1} is determined. From this the normal gradient q^{k+1} is determined using equation (32). This completes a time step and the procedure is reiterated.

SWWE formulation

The SWWE formulation follows quite closely the KGE formulation. The interior problem (28) is discretized as in (30):

$$[A]\{\zeta\}^{k+1} = \{b\}^k + \left\{\oint c^2\left(\frac{\theta}{2}(q^{k+1} + q^{k-1}) + (1 - \theta)q^k\right)\phi_i \, ds\right\}$$
$$- \oint \tau_0(H\mathbf{v})\cdot\hat{\mathbf{n}}\phi_i \, ds - \oint fh\mathbf{v}^k\cdot\hat{\mathbf{s}}\phi_i \, ds. \tag{34}$$

(The last two boundary integral terms have been pulled out of $\{b\}^k$ for clarity). The discretization of the RBC is as above, leading to

$$[A]\{\zeta\}^{k+1} + \oint \frac{c^2\theta}{1+f\varepsilon\Delta t}\,\zeta^{k+1}\left(\frac{p_0}{c\Delta t} + \frac{p_0\varepsilon\Delta t f^2}{2c} + \frac{1+f\varepsilon\Delta t}{4r}\right)\phi_i\,\mathrm{d}s$$
$$= \{b\}^k + \oint \frac{c^2}{1+f\varepsilon\Delta t}\left[[1-\theta+f(\varepsilon-\theta)\Delta t]q^k + \theta q^{k-1}\right.$$
$$+ \theta\zeta^k\left(\frac{2p_0}{c\Delta t} - \frac{p_0(1-\varepsilon)\Delta t f^2}{c} - \frac{f(1-\varepsilon)\Delta t}{2r}\right) - \theta\zeta^{k-1}\left(\frac{p_0}{c\Delta t} + \frac{p_0\varepsilon\Delta t f^2}{2c} - \frac{1-f\varepsilon\Delta t}{4r}\right)\Bigg]\phi_i\,\mathrm{d}s$$
$$- \oint \frac{\theta c^3 p_2\Delta t}{1+f\varepsilon\Delta t}\frac{\partial\zeta^k}{\partial s}\frac{\partial\phi_i}{\partial s}\,\mathrm{d}s - \oint \tau_0(H\mathbf{v})\cdot\hat{\mathbf{n}}\phi_i\,\mathrm{d}s - \oint fh\mathbf{v}^k\cdot\hat{\mathbf{s}}\phi_i\,\mathrm{d}s. \tag{35}$$

As in the KGE formulation, the first step in the solution procedure is the determination of ζ^{k+1} from (35). Following this, we determine q^{k+1} using equation (32). Then we compute $\mathbf{v}^{k+1}$ following the procedure outlined in the next subsection, which completes the time step.

Velocities

For the determination of the velocities we follow e.g. Werner and Lynch.[18] The x- and y-momentum equations (2) and (3) are approximated as

$$\left(\frac{u^{k+1}-u^k}{\Delta t}\right) - f\left(\frac{v^{k+1}+v^k}{2}\right) = -g\nabla_x\left(\frac{\zeta^{k+1}+\zeta^k}{2}\right), \tag{36}$$

$$\left(\frac{v^{k+1}-v^k}{\Delta t}\right) + f\left(\frac{u^{k+1}+u^k}{2}\right) = -g\nabla_y\left(\frac{\zeta^{k+1}+\zeta^k}{2}\right). \tag{37}$$

Rearrangement yields the system of equations

$$\begin{pmatrix} 2/\Delta t & -f \\ f & 2/\Delta t \end{pmatrix}\begin{pmatrix} u^{k+1} \\ v^{k+1} \end{pmatrix} = \begin{pmatrix} (2/\Delta t)u^k + fv^k - g\nabla_x(\zeta^{k+1}+\zeta^k) \\ -fu^k + (2/\Delta t)v^k - g\nabla_y(\zeta^{k+1}+\zeta^k) \end{pmatrix}, \tag{38}$$

which is easily solved using a Galerkin procedure. Hence the velocities at each node depend only on the elevation gradients at the respective node and can be recovered after the elevation has been computed via a relatively simple process. For the SWWE this must be done at the end of each time step. It should be noted that in this formulation no additional RBC is necessary for the velocities.

TEST CASES

The test cases are similar to the case from Reference 13 and consist of an initially Gaussian-shaped free surface centred about the position (x_0, y_0) on a two-dimensional mesh. The initial conditions are given by

$$\zeta(t=0, x, y) = \zeta_0 \exp\left(-\frac{r_0^2}{L^2}\right), \tag{39}$$

$$\frac{\partial\zeta}{\partial r}(t=0, x, y) = -\frac{2\zeta_0 r_0}{L^2}\exp\left(-\frac{r_0^2}{L^2}\right), \tag{40}$$

where $\zeta_0 = 1$ m is an amplitude, $r_0^2 = (x - x_0)^2 + (y - y_0)^2$ and $L = 25$ km is a length scale. Two time levels of ζ are initialized as above and the initial conditions for the velocities are $\mathbf{v}^k = 0$. For the Klein–Gordon equation cases the potential vorticity Q' is obtained from the initial conditions on ζ and $\mathbf{v}$ via equation (8). The gravitational acceleration is $g = 9{\cdot}81$ m s^{-2} and the wave speed is $c = 22{\cdot}15$ m s^{-1} (corresponding to a water depth $h = 50$ m). The mesh size in all cases was set to $\Delta s = 3{\cdot}75$ km and the Courant number is set to $Co = c\Delta t/\Delta s = 0{\cdot}25$, leading to a time step of $\Delta t = 42{\cdot}3$ s, since preliminary testing showed that for such a small Courant number the results are independent of the time step chosen.

In the first test case we use a circular mesh (Figure 3) consisting of 2521 nodes and 4800 triangular finite elements, which has a diameter of 300 km. The radial spacing is $\Delta r = 3{\cdot}75$ km and the circumferential spacing is $\Delta\Theta = 2\pi\Delta r/12r$. The location of the reference nodes is given in Table I. In the first set of runs the initial distribution is centred about the origin ($x_0 = y_0 = 0$).

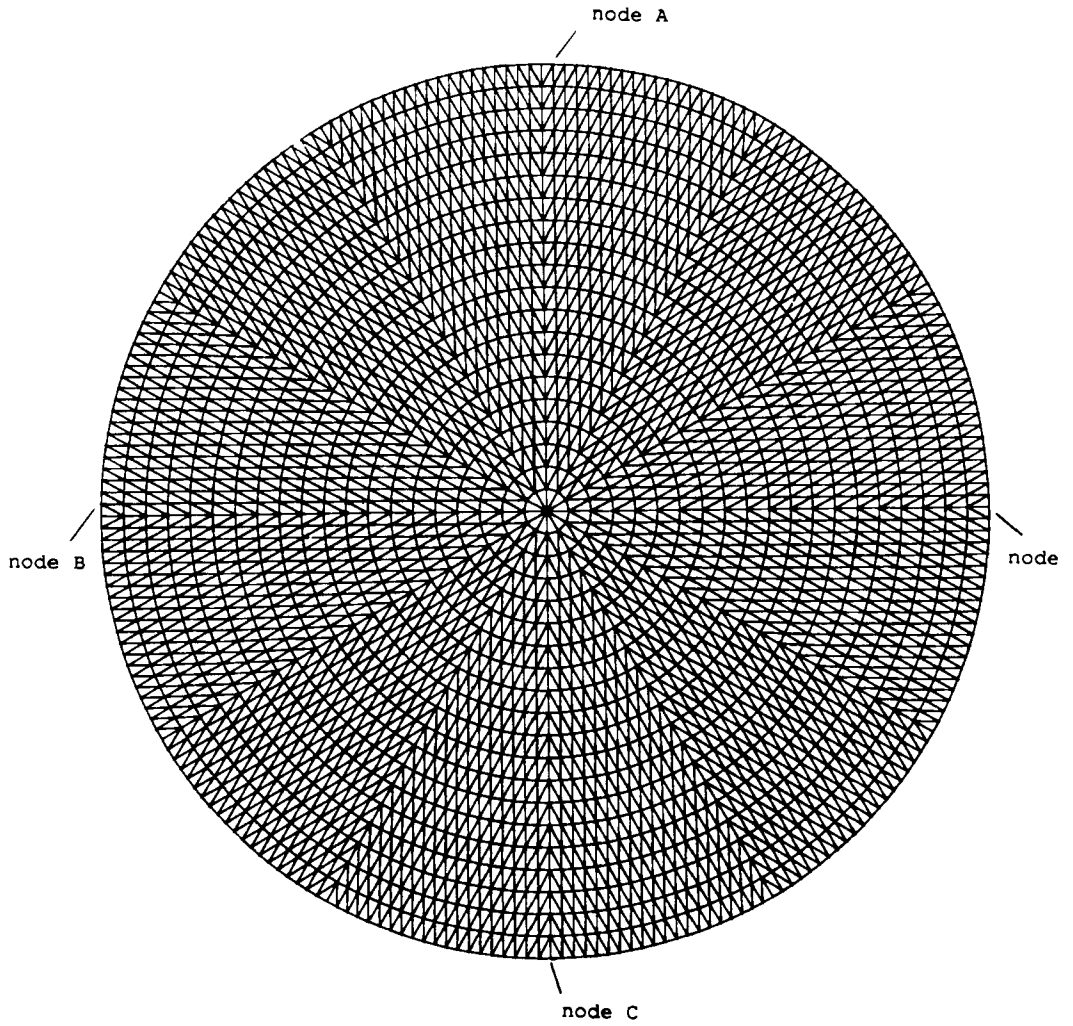

Figure 3. Circular two-dimensional finite element mesh used for the study of radiation boundary conditions, indicating also the location of the reference nodes

Table I. Location of reference nodes A–D in the circular mesh

Node	x (km)	y (km)
A	0	150
B	−150	0
C	0	−150
D	150	0

This is a somewhat idealized case, since the curvatures of the wave front and of the boundary are the same, leading effectively to one-dimensional wave propagation at the boundary. Hence in a second set of runs the initial distribution is uncentred, where the results are shown for the parameters $x_0 = 60$ km and $y_0 = 30$ km.

The second test case consists of a rectangular mesh (Figure 4) with 14,661 nodes and 28,800 triangular finite elements. The mesh has the dimensions 675 × 300 km^2, centred about the origin. The location of the reference nodes is given in Table II. In this test case we can investigate the

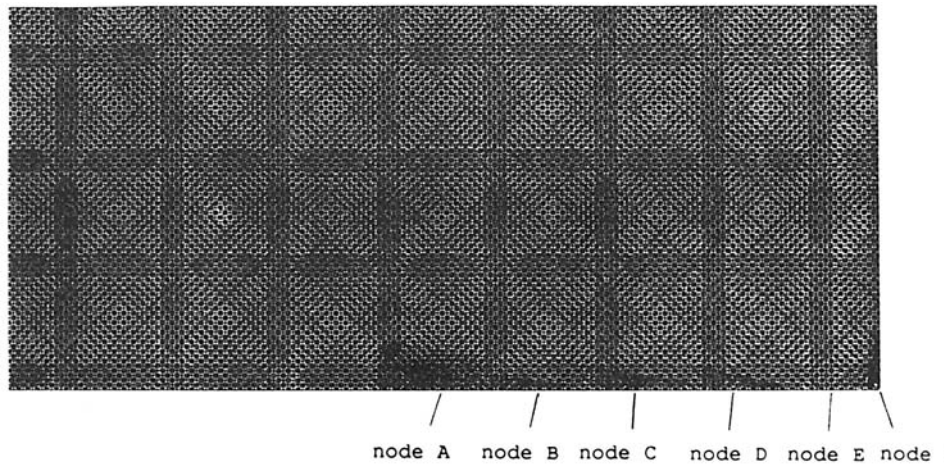

Figure 4. Rectangular two-dimensional finite element mesh used for the study of radiation boundary conditions, indicating also the location of the reference nodes

Table II. Location of the reference nodes A–F in the rectangular mesh

Node	x (km)	y (km)
A	0	−150
B	75	−150
C	150	−150
D	225	−150
E	300	−150
F	337.5	−150

influence of a relative curvature between a wave front and the boundary and a varying angle of incidence of the wave front. The corner nodes are particularly interesting, since the relative curvature is poorly resolved.

In all cases the results for these meshes are shown in comparison with extended, otherwise identical meshes (with a second-order RBC imposed on the boundary of the extended mesh). This allows for the testing of the effect of the boundary condition alone, since it is the only difference between the two runs. The results are shown for the above-derived second-order RBC with Padé coefficients ($p_0 = 1{\cdot}0, p_2 = 0{\cdot}5$) as well as for the first-order RBC with a Padé coefficient ($p_0 = 1{\cdot}0$) and for the Sommerfeld RBC. The time-weighting factors θ and ε in the boundary integral are chosen to be $\theta = \varepsilon = 0{\cdot}5$. Preliminary testing showed that the results are independent of θ for $\theta \geq 0{\cdot}5$ and the solutions became unstable for $\theta < 0{\cdot}5$. In all cases the interior problem is solved with an explicit approach to the wave equation operator as in Reference 15. All domain and boundary integrals are evaluated by nodal quadrature; as a consequence, all mass matrices are diagonalized.

As an approximate measure for the quality of the boundary condition we determine a maximum relative error after

$$\text{max.rel.error} = \frac{\max(\Delta\zeta)}{\max(\zeta)}, \tag{41}$$

where $\Delta\zeta$ is the discrepancy induced by the boundary condition compared with an extended mesh solution.

RESULTS

We examine first the pure wave equation results, i.e. $f = 0$, in order to focus on the curvature effects. We then introduce rotation and examine the KGE and SWWE cases.

Wave equation

Figures 5(a) and 5(b) show the time history of the elevation at node A in the circular mesh for the Sommerfeld RBC and the second-order RBC for the centred initial condition ($x_0 = y_0 = 0$). Figures 6(a) and 6(b) show the wave equation solution at nodes A–D for the two boundary conditions for the uncentred initial distribution ($x_0 = 60$ km, $y_0 = 30$ km). The solution subject to the second-order RBC shows a clear improvement over the Sommerfeld RBC. Figure 7 shows a perspective plot of the 2D wave equation solution for the uncentred case using the second-order RBC. Shown are the elevations for the first $350\Delta t$ in $25\Delta t$ increments (upper left to lower right).

Figures 8(a) and 8(b) show the time history of the elevation at nodes A–F along the boundary of the rectangular mesh as compared with the extended mesh for the two boundary conditions applied for the 'pure' wave equation. The maximum relative error compared with the extended mesh solution following equation (42) is shown in Figure 9. The plots show the superior performance of the second-order RBC as compared with the Sommerfeld RBC. For both RBCs the results are best at normal incidence. Along the straight boundary the Sommerfeld RBC is lacking a term that accounts for a relative curvature between wave front and boundary (the $\partial^2\zeta/\partial s^2$ term in the second-order RBC). The plots clearly indicate that the inclusion of this term significantly improves the results for even small amounts of relative curvature (near node A).

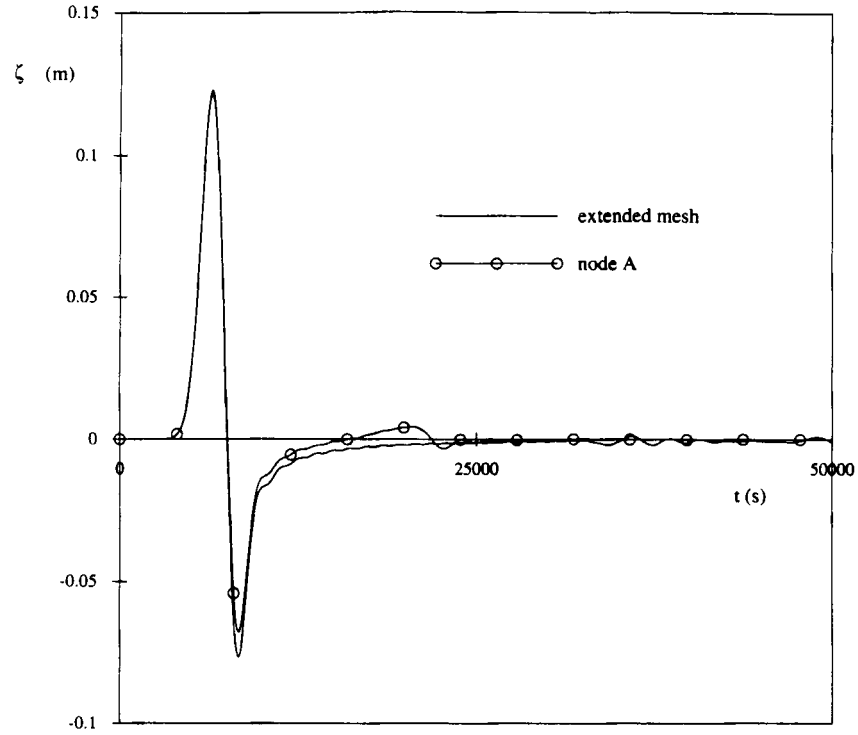

Figure 5(a). Elevations at node A for the wave equation on the circular mesh; comparison between Sommerfeld RBC and extended mesh results ($x_0 = y_0 = 0$)

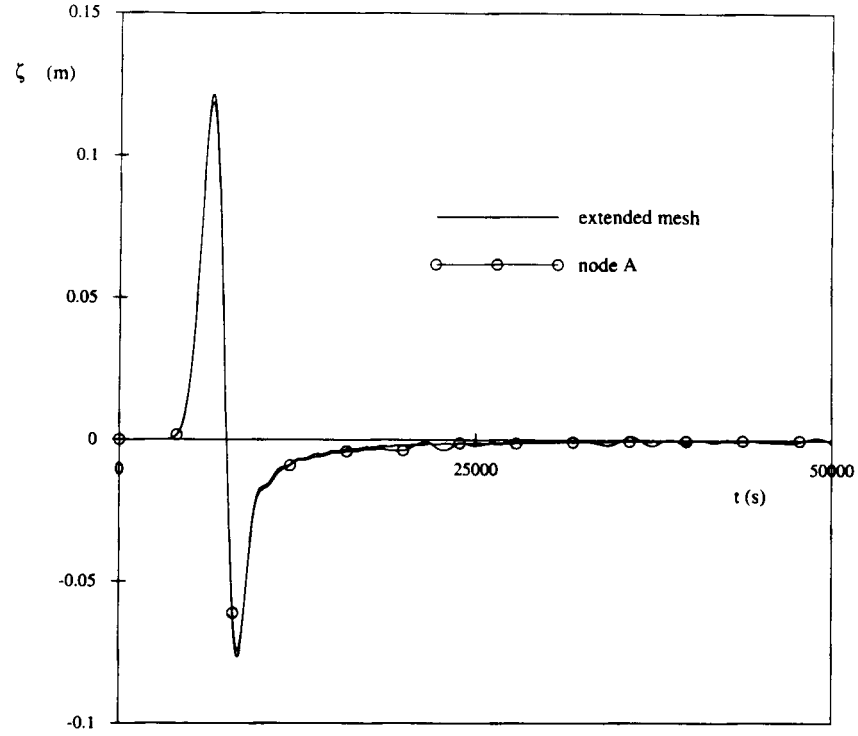

Figure 5(b). Elevations at node A for the wave equation on the circular mesh; comparison between second-order RBC and extended mesh results ($x_0 = y_0 = 0$)

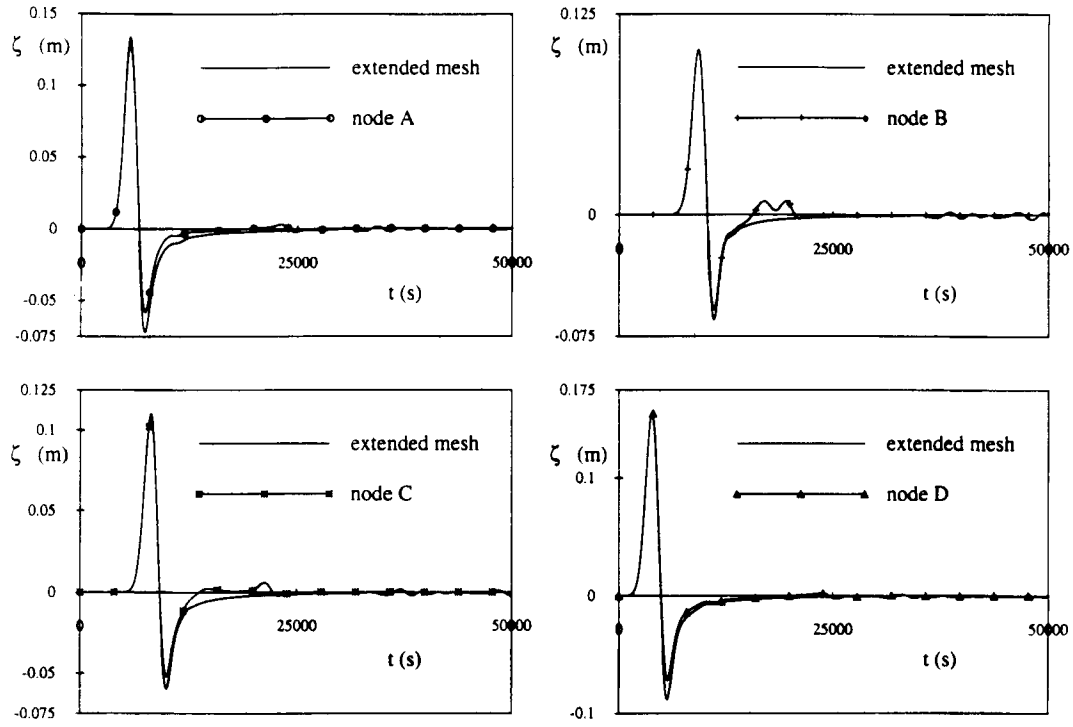

Figure 6(a). Elevations at nodes A–D for the wave equation on the circular mesh; comparison between Sommerfeld RBC and extended mesh results ($x_0 = 60$ km, $y_0 = 30$ km)

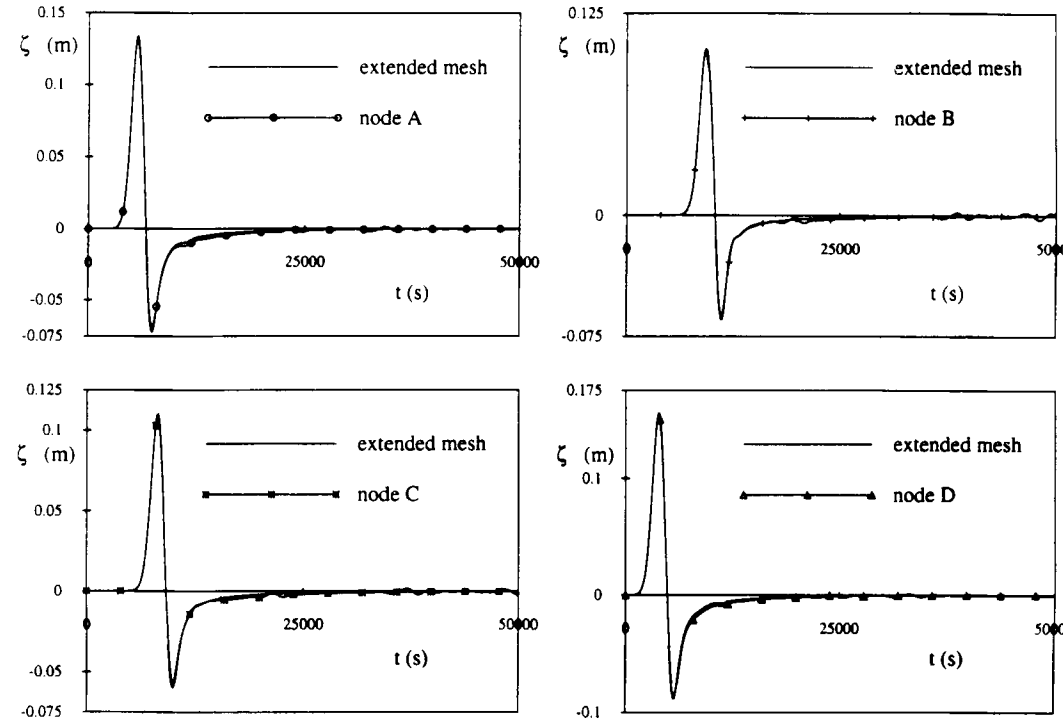

Figure 6(b). Elevations at nodes A–D for the wave equation on the circular mesh; comparison between second-order RBC and extended mesh results ($x_0 = 60$ km, $y_0 = 30$ km)

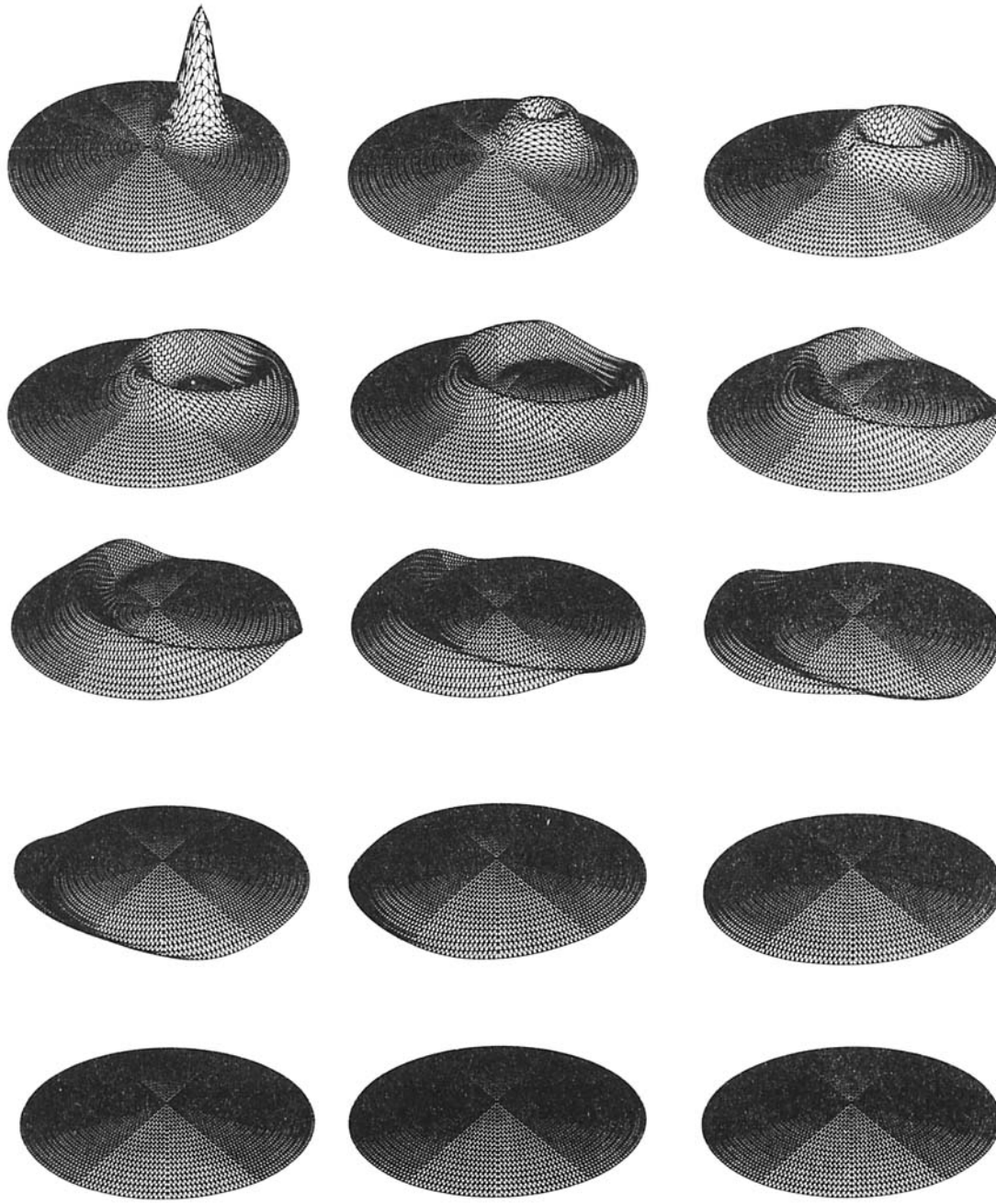

Figure 7. Perspective plot of the elevation field for the 2D wave equation using the second-order RBC for increasing time (upper left to lower right). Shown are the elevations for the first $350\Delta t$ in $25\Delta t$ increments

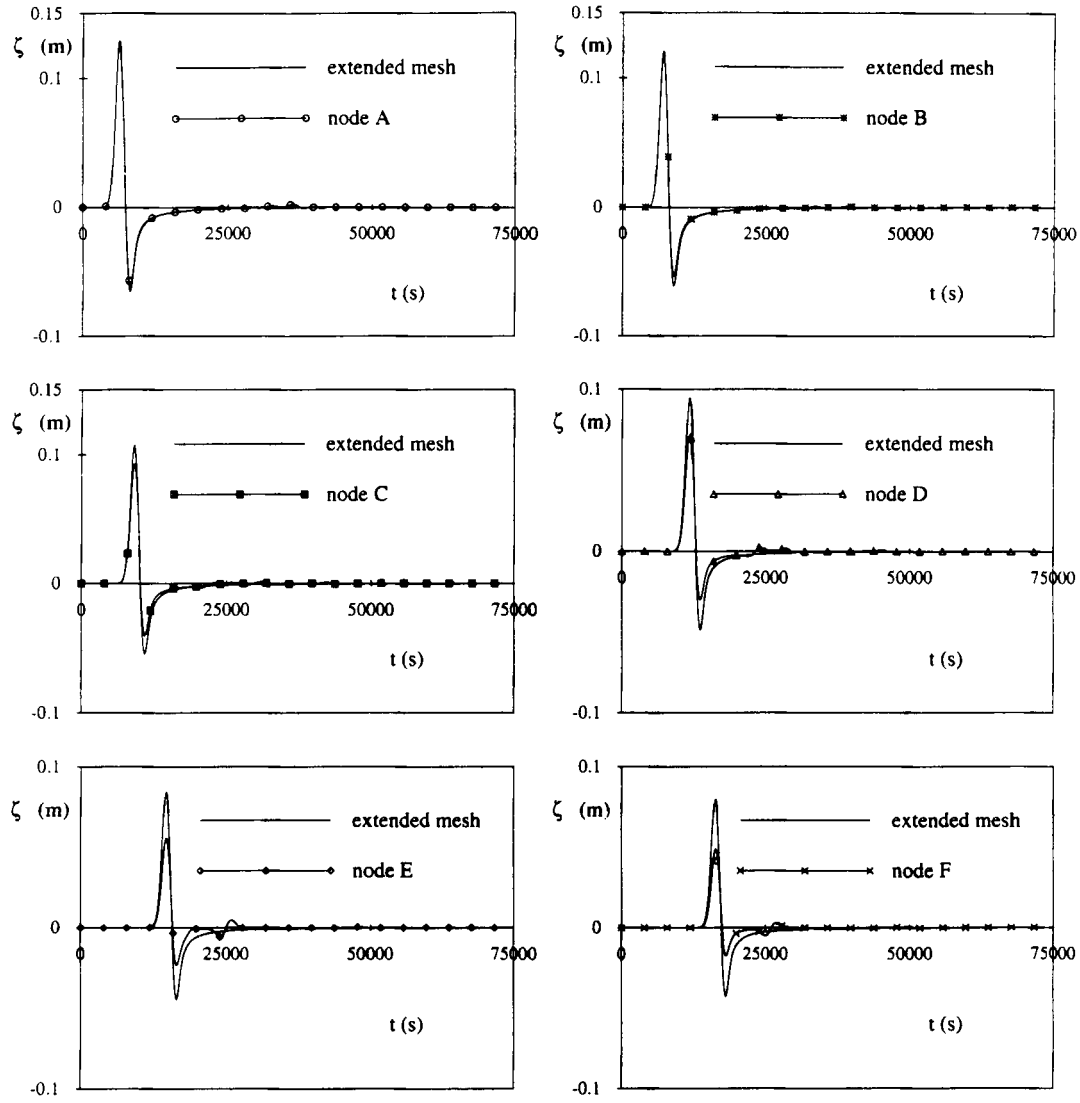

Figure 8(a). Elevations at nodes A–F for the wave equation on the rectangular mesh; comparison between Sommerfeld RBC and extended mesh results

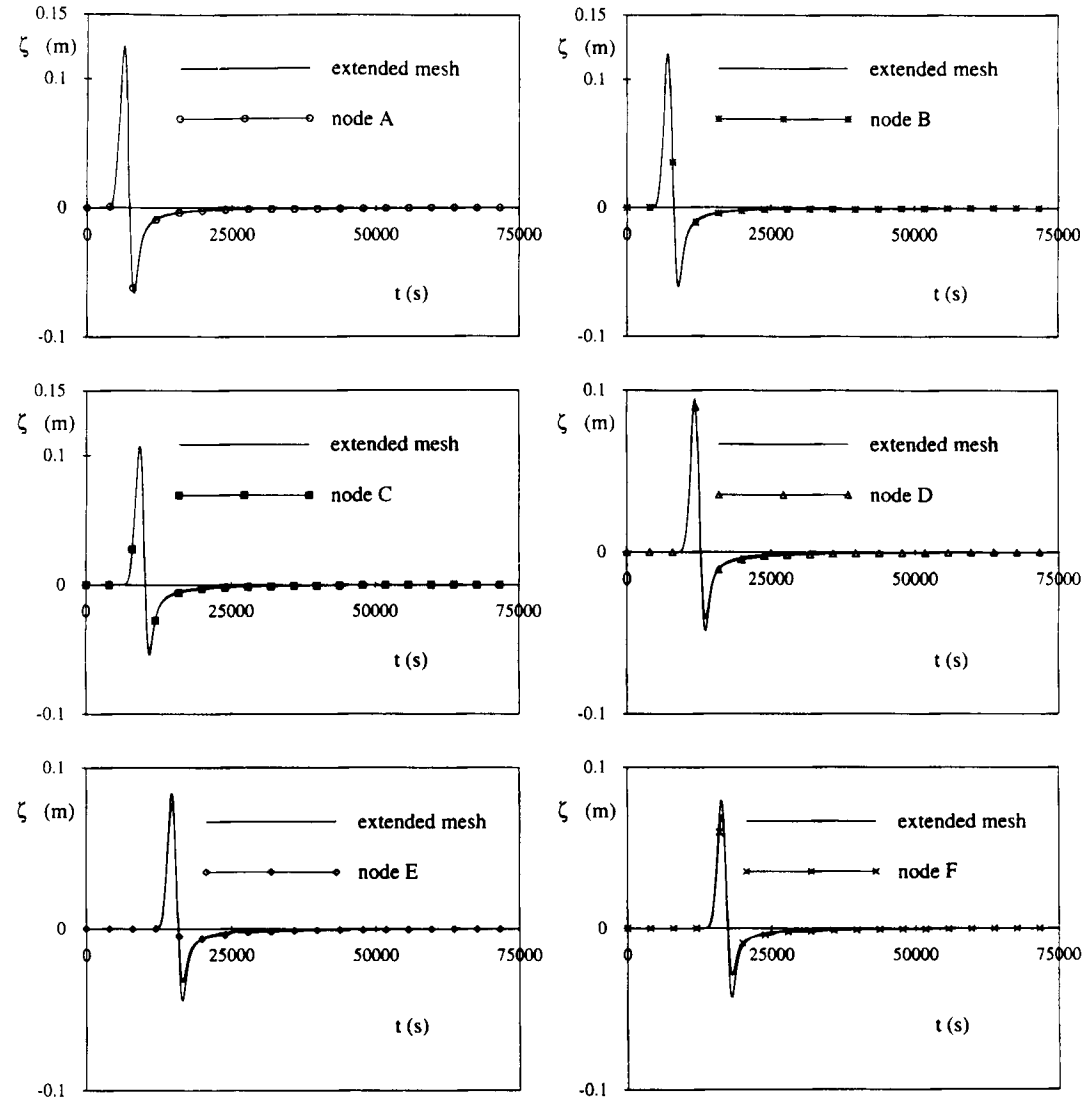

Figure 8(b). Elevations at nodes A–F for the wave equation on the rectangular mesh; comparison between second-order RBC and extended mesh results

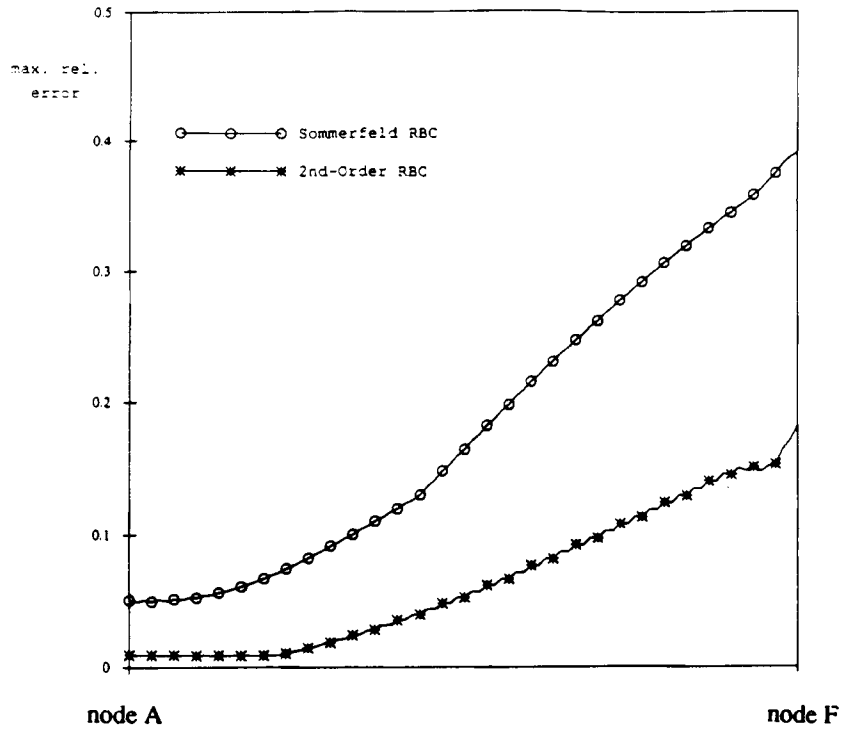

Figure 9. Maximum relative error along the boundary of the rectangular mesh for various boundary conditions in comparison with an extended mesh solution for the wave equation

KGE formulation

Figures 10(a) and 10(b) show the time history of the elevation at nodes A–F along the boundary of the rectangular mesh as compared with the extended mesh for the two boundary conditions applied for the shallow water wave equations in the KGE formulation. Figure 11 shows the maximum relative error following equation (42) along the boundary. As can be seen in these plots, the second-order RBC again shows a superior performance as compared with the Sommerfeld RBC. The plots also reveal that the extended mesh results show reflections from the boundary which travel through the system. These reflections are mainly responsible for the relatively poor performance of the second-order RBC near normal incidence and they also show that extending the mesh alone does not necessarily improve the results.

For the case of the KGE formulation using the second-order RBC we also present velocity solutions. Figure 12 shows the complete velocity field at $t = 60{,}000$ s. At this time the initial disturbance has almost completely left the computational domain and we can see the set-up of a clockwise gyre. Figure 13 shows the velocities at (a) node A and (b) node F versus time in comparison with an extended mesh solution. The comparison of the velocities with the extended mesh is excellent for the passing of the initial disturbance (which is wave-equation-dominated) and still quite good for the later period (which is dominated by the rotational term in the momentum equations) at node A. At the corner node F the comparisons are still quite reasonable.

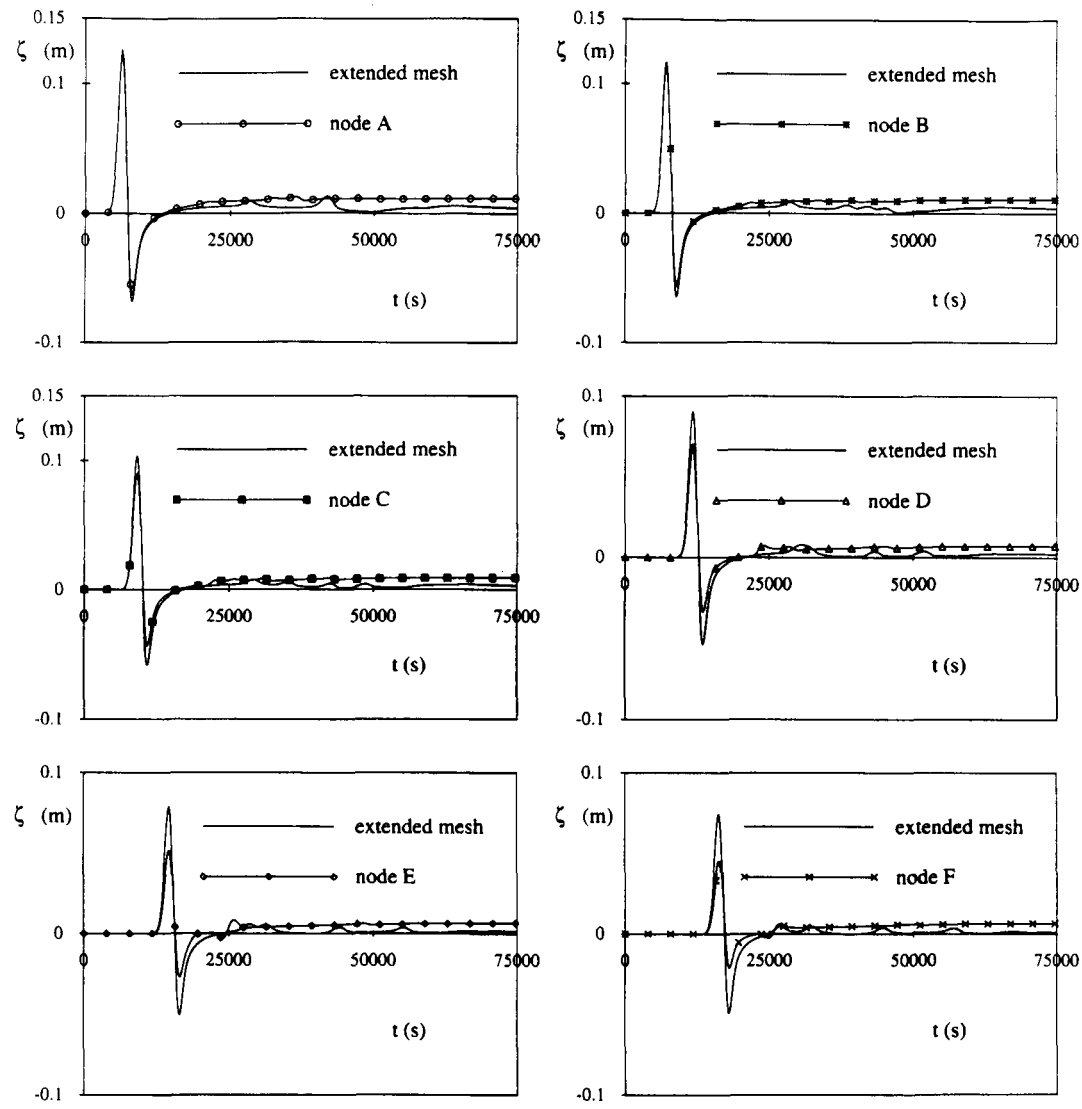

Figure 10(a). Elevations at nodes A–F for the KGE formulation on the rectangular mesh; comparison between Sommerfeld RBC and extended mesh results

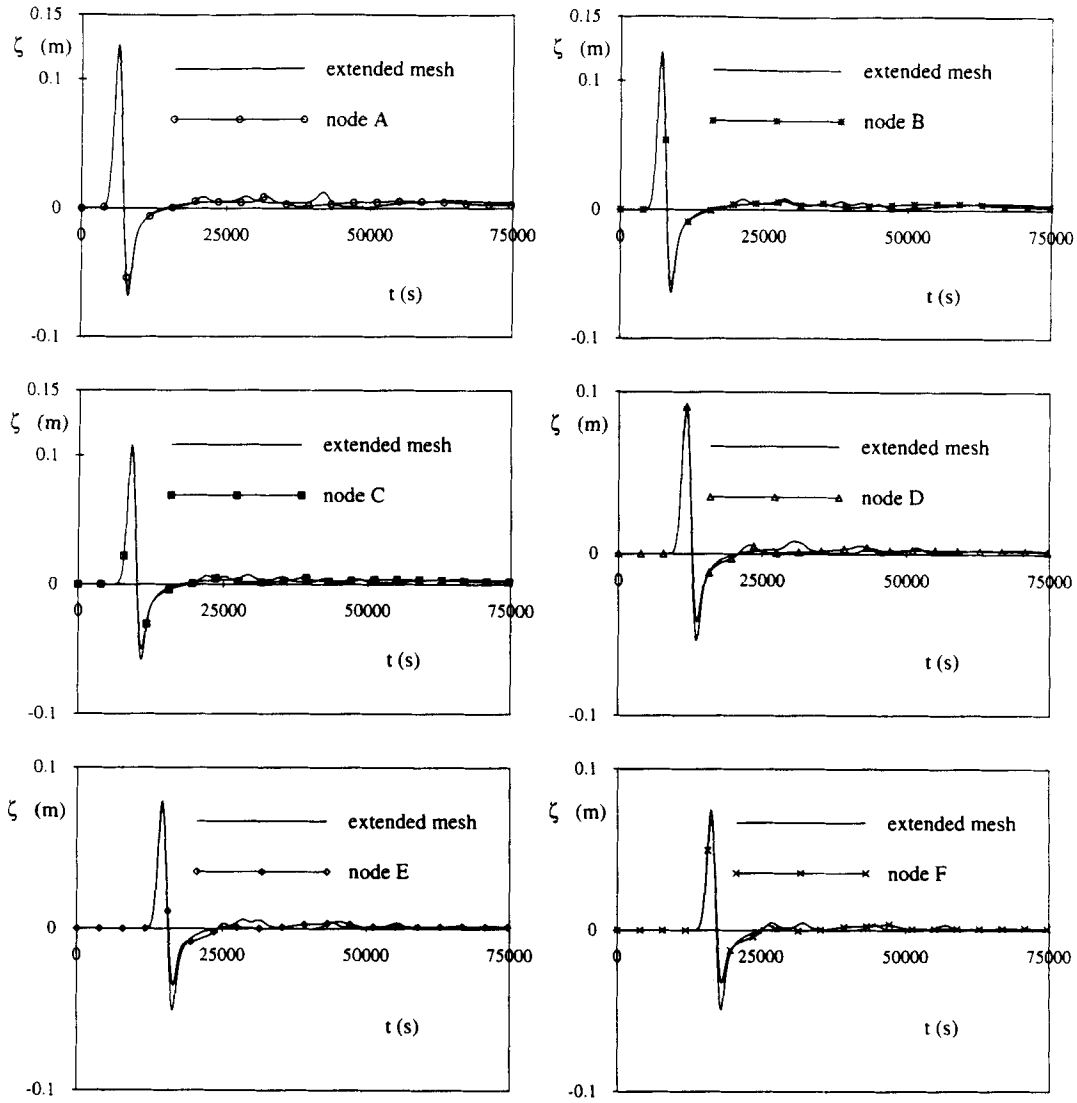

Figure 10(b). Elevations at nodes A–F for the KGE formulation on the rectangular mesh; comparison between second-order RBC and extended mesh results

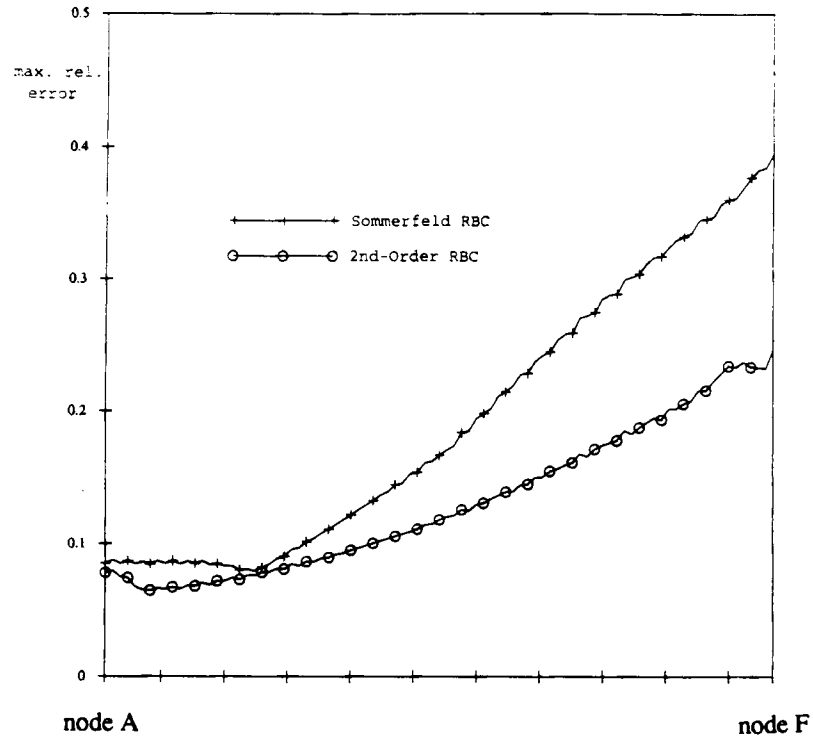

Figure 11. Maximum relative error along the boundary of the rectangular mesh for various boundary conditions in comparison with an extended mesh solution for the KGE formulation

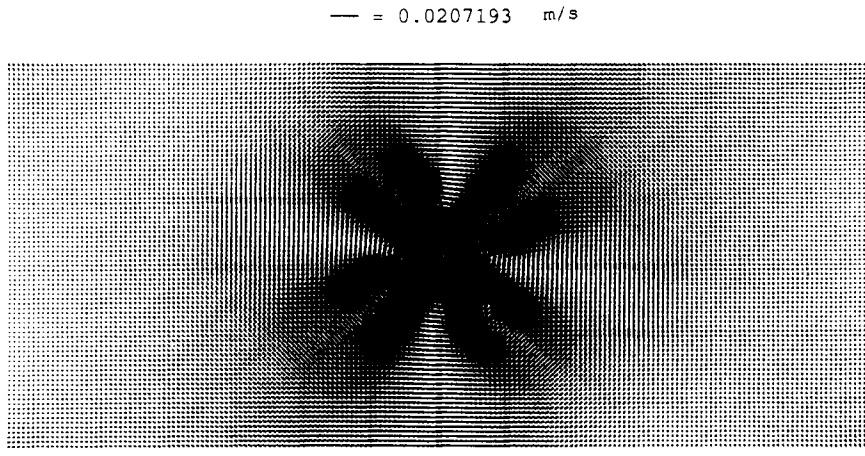

Figure 12. Velocity field for the KGE formulation using the second-order RBC on the rectangular mesh at $t = 60{,}000$ s

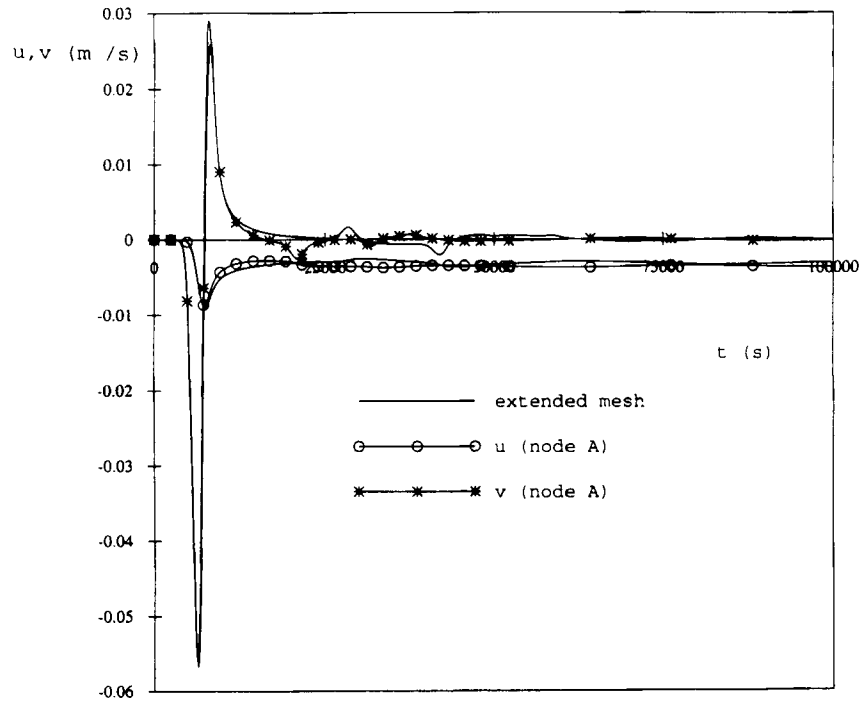

Figure 13(a). Velocities at node A for the KGE formulation on the rectangular mesh using the second-order RBC in comparison with an extended mesh solution

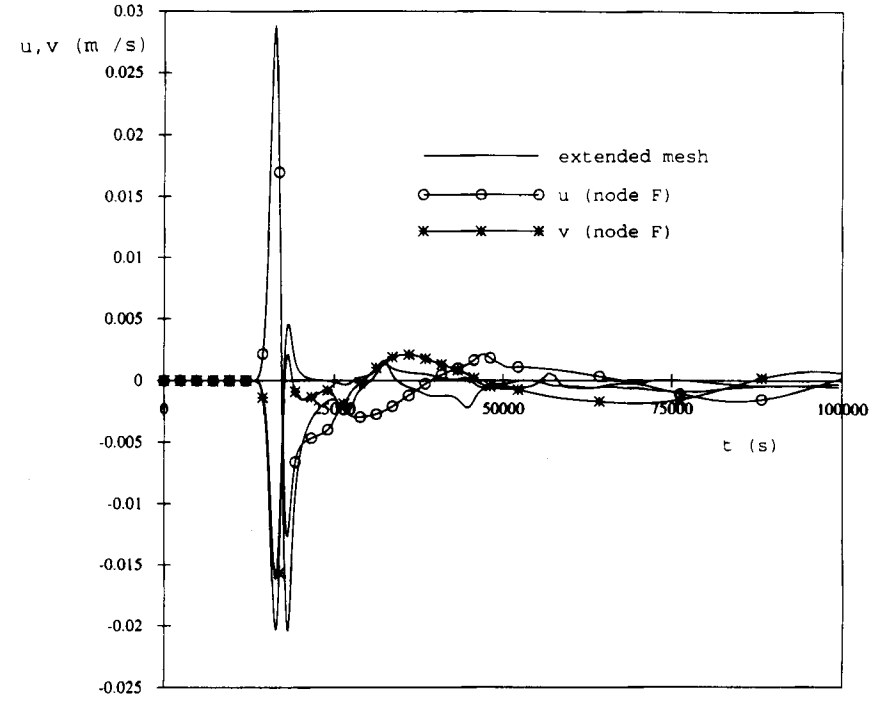

Figure 13(b). Velocities at node F for the KGE formulation on the rectangular mesh using the second-order RBC in comparison with an extended mesh solution

SWWE formulation

In Figures 14–17 we show the same plots for the SWWE formulation that were presented in Figures 10–13 for the KGE formulation. The figures show that the time history of the elevations and velocities and the quality of the boundary conditions in terms of agreement with the extended mesh results are virtually identical with the results obtained for the KGE formulation. This demonstrates the validity of the RBC approach for the SWWE formulation.

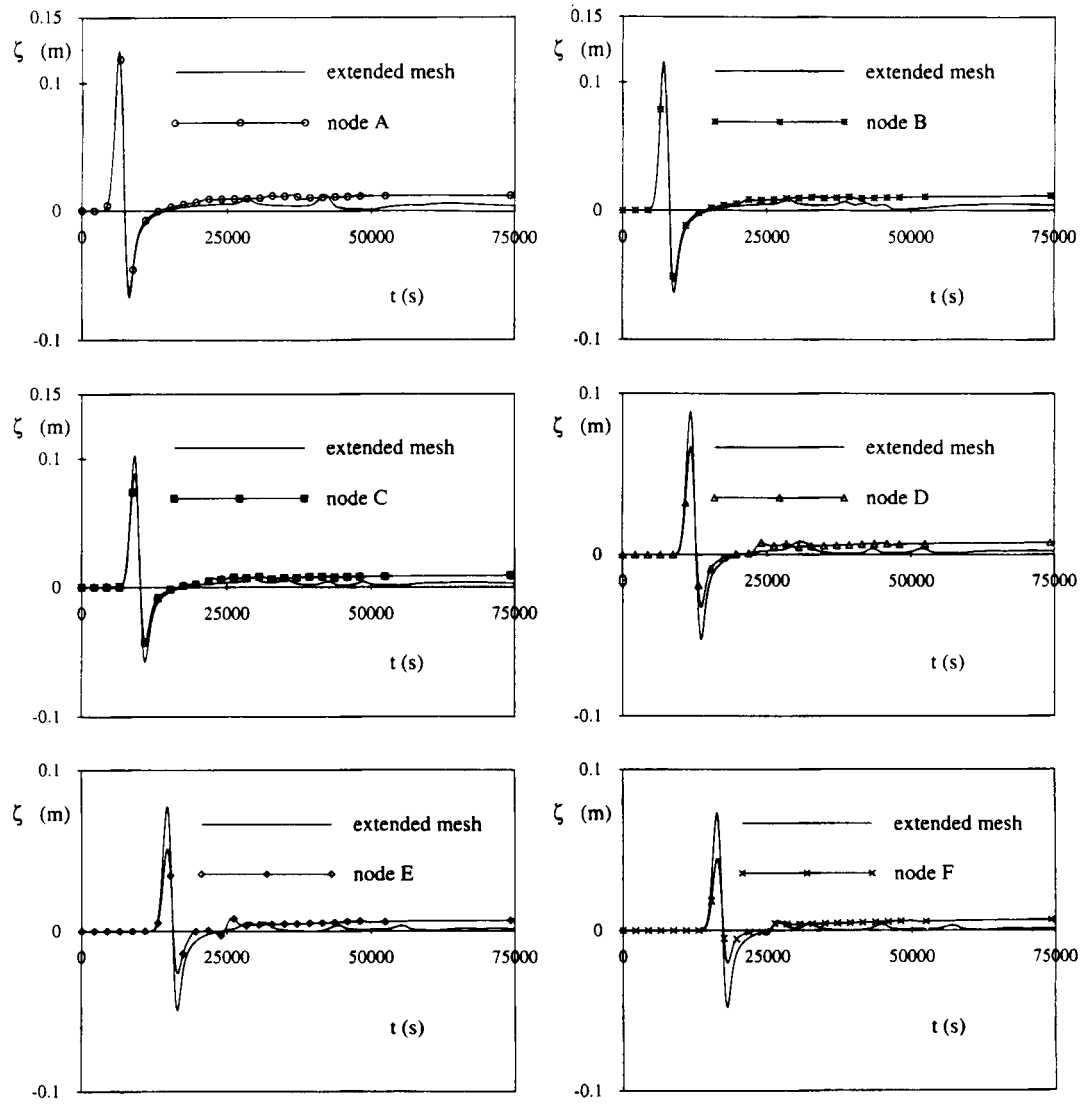

Figure 14(a). Elevations at nodes A–F for the SWWE formulation on the rectangular mesh; comparison between Sommerfeld RBC and extended mesh results

In order to demonstrate the long-term stability of the code using this approach, Figure 17(c) shows the velocities at node F for an extended run. Here the simulation was run for $7{\cdot}5 \times 10^6$ s, which is roughly equivalent to 3 months. We can see that the velocities reach a stable steady state solution. Similar runs for the smaller circular mesh also showed no sign of distress for runs of more than a year of simulation time.

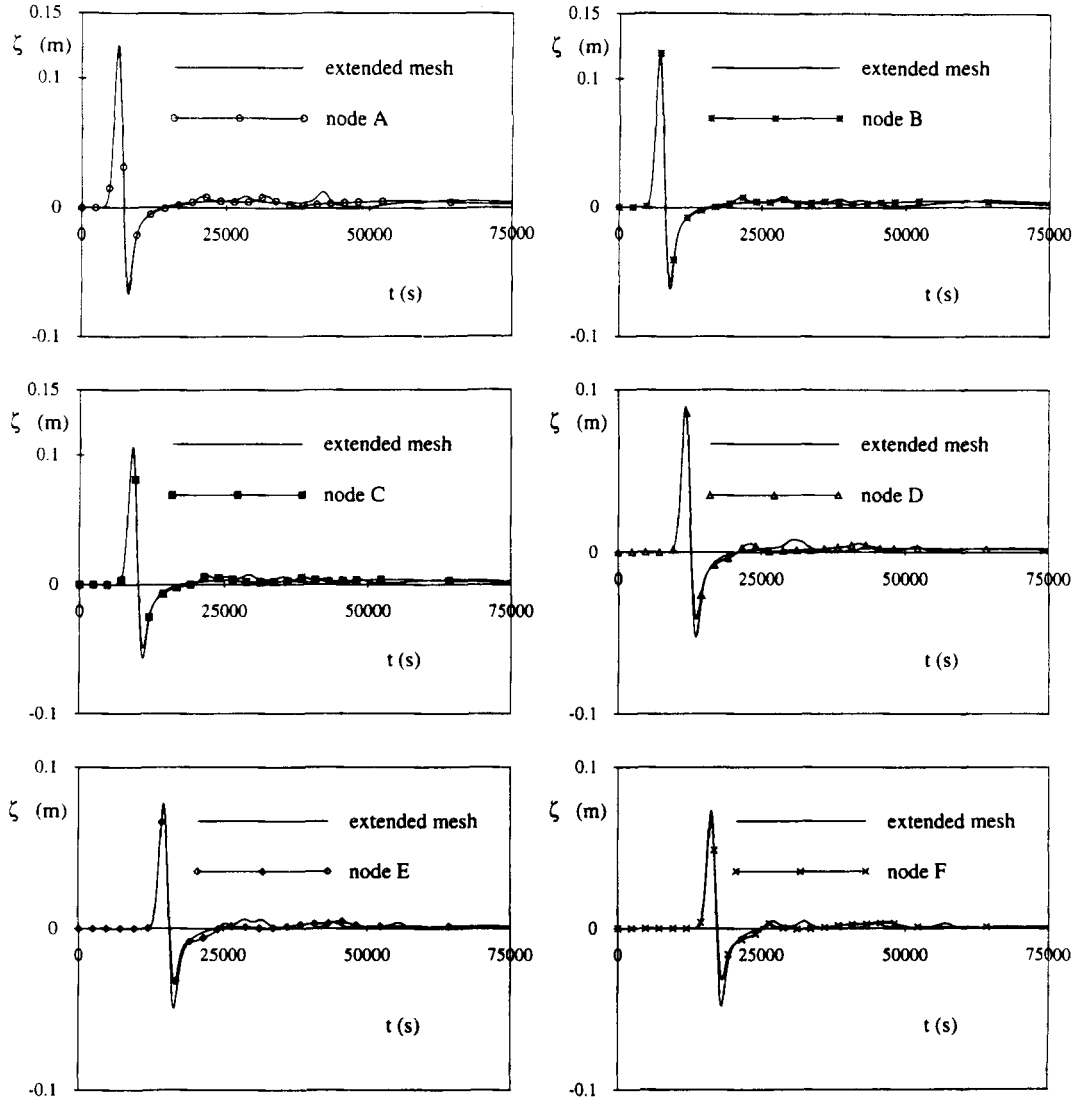

Figure 14(b). Elevations at nodes A–F for the SWWE formulation on the rectangular mesh; comparison between second-order RBC and extended mesh results

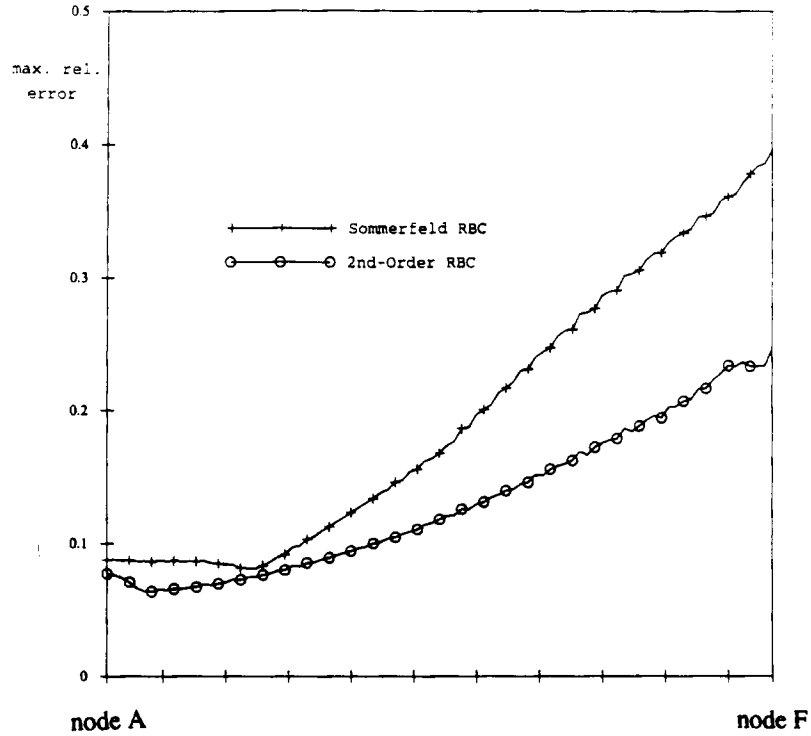

Figure 15. Maximum relative error along the boundary of the rectangular mesh for various boundary conditions in comparison with an extended mesh solution for the SWWE formulation

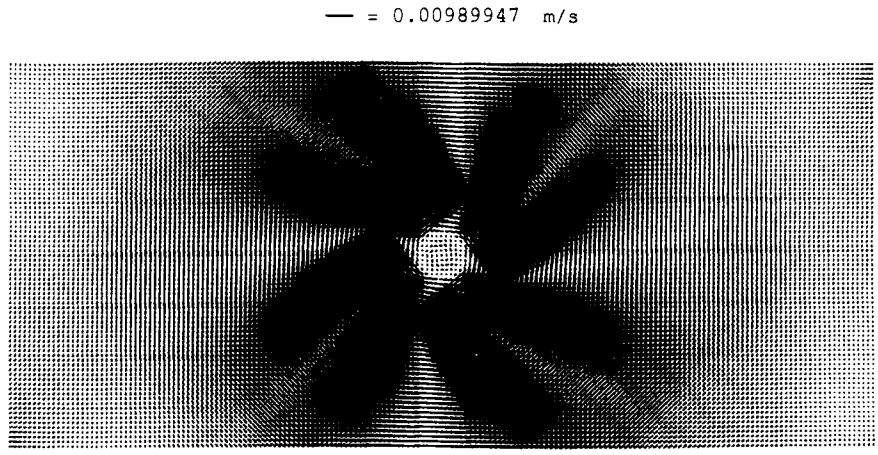

Figure 16. Velocity field for the SWWE formulation using the second-order RBC on the rectangular mesh at $t = 60{,}000$ s

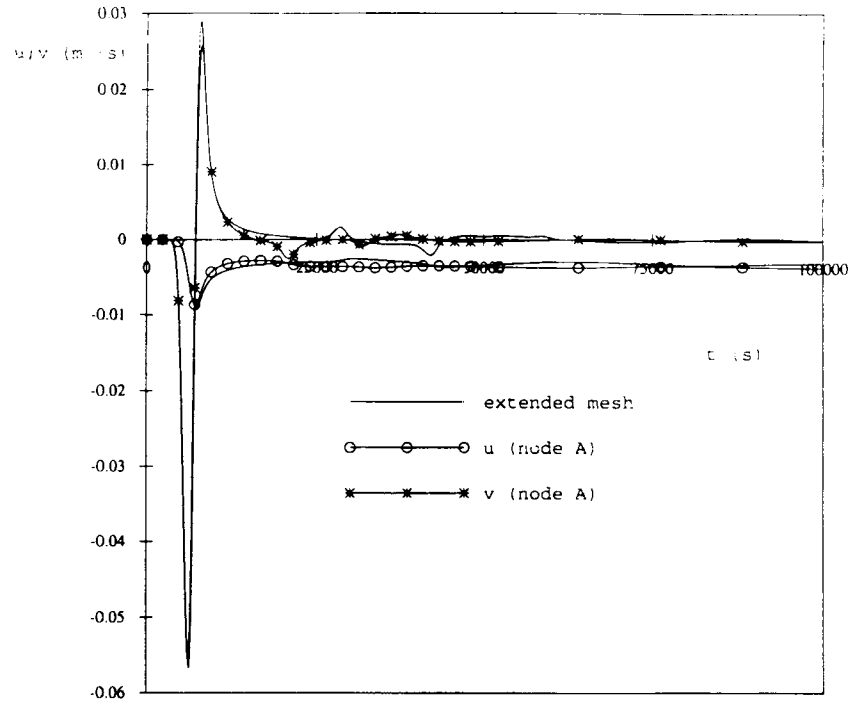

Figure 17(a). Velocities at node A for the SWWE formulation on the rectangular mesh using the second-order RBC in comparison with an extended mesh solution

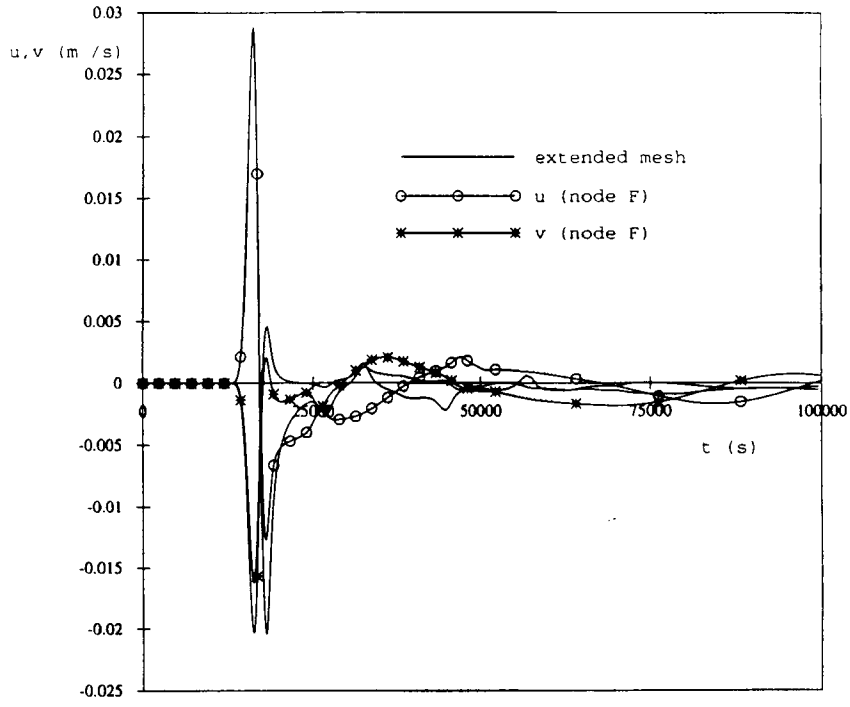

Figure 17(b). Velocities at node F for the SWWE formulation on the rectangular mesh using the second-order RBC in comparison with an extended mesh solution

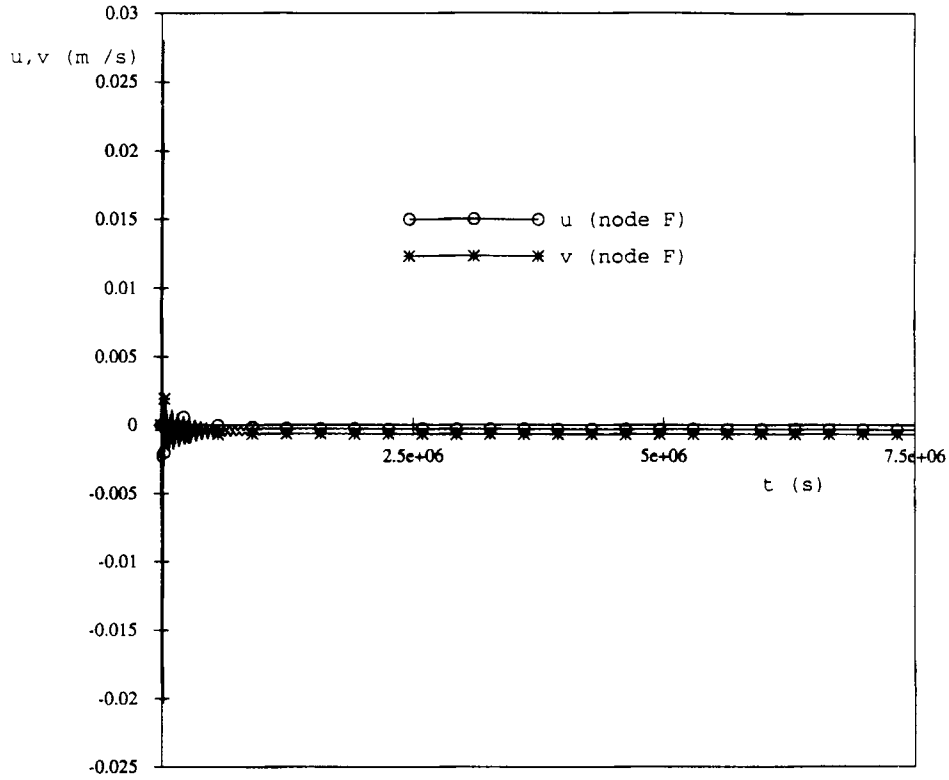

Figure 17(c). Velocities at node F for the SWWE formulation on the rectangular mesh using the second-order RBC—extended run (3 months)

CONCLUSIONS

The test cases show the validity of the second-order RBC for various meshes, in particular its superiority over the Sommerfeld RBC. The approach is valid for arbitrary, unstructured meshes and not restricted to certain geometries. The results also indicate certain guidelines for good results: in general it is advantageous to chose a boundary shape that avoids sharp kinks or corners and enables the waves to impinge on the boundary close to normal incidence.

The results for both the SWWE and KGE formulations in their simplest form are very encouraging and in good agreement with those for simpler 1D cases as studied in Reference 14. Further studies should concentrate on the effect of varying water depth and the inclusion of friction and wind forcing. A further challenge is the superposition of an RBC solution upon a motion with stronger boundary conditions, e.g. Dirichlet conditions on tidally induced elevation.

ACKNOWLEDGEMENT

This work was supported by the U.S. National Science Foundation, grant OCE-9012612.

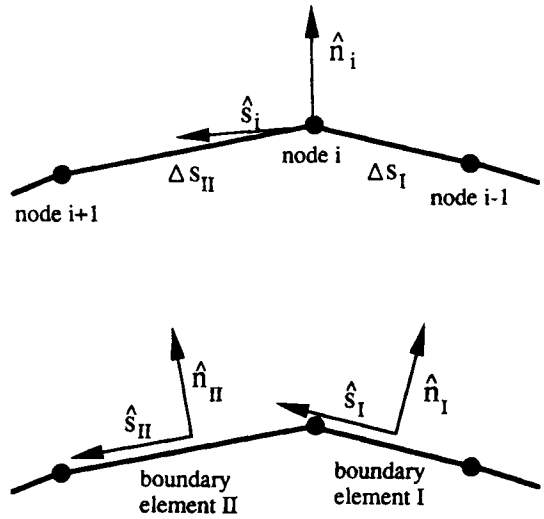

Figure 18. Notation of the normal and tangential unit vectors at an arbitrary boundary node

APPENDIX: EVALUATION OF BOUNDARY INTEGRALS

For the evaluation of the boundary integral of the second tangential derivative we apply a partial integration

$$\oint \left(\frac{\partial^2 \zeta}{\partial s^2}\right) \phi_i \, ds = -\oint \frac{\partial \zeta}{\partial s} \frac{\partial \phi_i}{\partial s} \, ds + \left[\frac{\partial \zeta}{\partial s} \phi_i\right]_{I}^{II}. \tag{42}$$

The second term on the right-hand side is zero, whereas the first term for linear basis and weighting functions is evaluated as

$$-\oint \frac{\partial \zeta}{\partial s} \frac{\partial \phi_i}{\partial s} \, ds = \frac{\zeta_{i+1} - \zeta_i}{\Delta s_{II}} - \frac{\zeta_i - \zeta_{i-1}}{\Delta s_I} \tag{43}$$

(see Figure 18). The boundary integral of the curvature term may be evaluated as[19]

$$\oint \frac{1}{r} \phi_i \, ds = \oint \frac{\partial \alpha}{\partial s} \phi_i \, ds = \oint \phi_i \, d\alpha = \Delta\alpha, \tag{44}$$

where

$$\sin(\Delta\alpha) = \hat{s}_I \times \hat{s}_{II}. \tag{45}$$

Hence we can deduce that in effect

$$\frac{1}{r} = \frac{\Delta\alpha}{\Delta s}. \tag{46}$$

REFERENCES

1. D. C. Chapman, 'Numerical treatment of cross-shelf open boundaries in a barotropic coastal ocean model', *J. Phys. Oceanogr.*, **15**, 1060–1075 (1985).

2. T. G. Moore, J. G. Blaschak, A. Taflove and G. A. Kriegsmann, 'Theory and application of radiation boundary operators', *IEEE Trans. Anten. Propagat.*, **AP-36**, 1797–1812 (1988).
3. D. Givoli, 'Non-reflecting boundary conditions', *J. Comput. Phys.*, **94**, 1–29 (1991).
4. P. Bettess, 'Infinite elements', *Int. J. Numer. Methods Eng.*, **11**, 53–64 (1977).
5. D. R. Lynch, K. P. Paulsen and J. W. Strohbehn, 'Hybrid element method for unbounded electromagnetic problems in hyperthermia', *Int. J. Numer. Methods Eng.*, **23**, 1915–1937 (1986).
6. R. W. Ziolkowski, N. K. Madsen and R. C. Carpenter, 'Three-dimensional computer modelling of electromagnetic fields: a global lookback lattice truncation scheme', *J. Comput. Phys.*, **50**, 360–408 (1983).
7. A. Sommerfeld, *Partial Differential Equations in Physics*, Academic Press, New York, 1949.
8. I. Orlanski, 'A simple boundary condition for unbounded hyperbolic flows', *J. Comput. Phys.*, **21**, 251–269 (1976).
9. B. Engquist and A. Majda, 'Absorbing boundary conditions for the numerical simulation of waves', *Math. Comput.*, **31**, 629–651 (1977).
10. A. Bayliss and E. Turkel, 'Radiation boundary conditions for wave-like equations', *Commun. Pure Appl. Math.*, **33**, 707–725 (1980).
11. K. Feng, 'Finite element method and natural boundary reduction', *Proc. Int. Congr. Mathematicians*, Warszawa, 1983.
12. R. L. Higdon, 'Numerical absorbing boundary conditions for the wave equation', *Math. Comput.*, **49**, 65–90 (1987).
13. G. K. Verboom and A. Slob, 'Weakly-reflective boundary conditions for two-dimensional shallow water flow problems', *Adv. Water Resources*, **7**, 192–197 (1984).
14. M. Johnsen, K. D. Paulsen and F. E. Werner, 'Radiation boundary conditions for finite element solutions of generalized wave equations', *Int. J. Numer. Methods Fluids*, **12**, 765–783 (1991).
15. D. R. Lynch and W. G. Gray, 'A wave equation model for finite element tidal computations', *Comput. Fluids*, **7**, 207–228 (1979).
16. A. E. Gill, *Atmosphere–Ocean Dynamics*, Academic Press, San Diego, CA, 1982.
17. I. P. E. Kinnmark and W. G. Gray, 'A generalized wave equation formulation of tidal circulation', in C. Taylor (ed.), *Proc. 4th Int. Conf. on Numerical Methods in Laminar and Turbulent Flows*, Pineridge, Swansea, 1985, pp. 1312–1324.
18. F. E. Werner and D. R. Lynch, 'Field verification of wave equation tidal dynamics in the English Channel and southern North Sea', *Adv. Water Resources*, **10**, 115–130 (1987).
19. J. M. Sullivan, D. R. Lynch and K. O'Neill, 'Finite element simulation of planar instabilities during solidification of an undercooled melt, *J. Comput. Phys.*, **69**, 81–110 (1987).